Resource

Cell Reports

Single-Cell Telomere-Length Quantification Couples Telomere Length to Meristem Activity and Stem Cell Development in *Arabidopsis*

Graphical Abstract

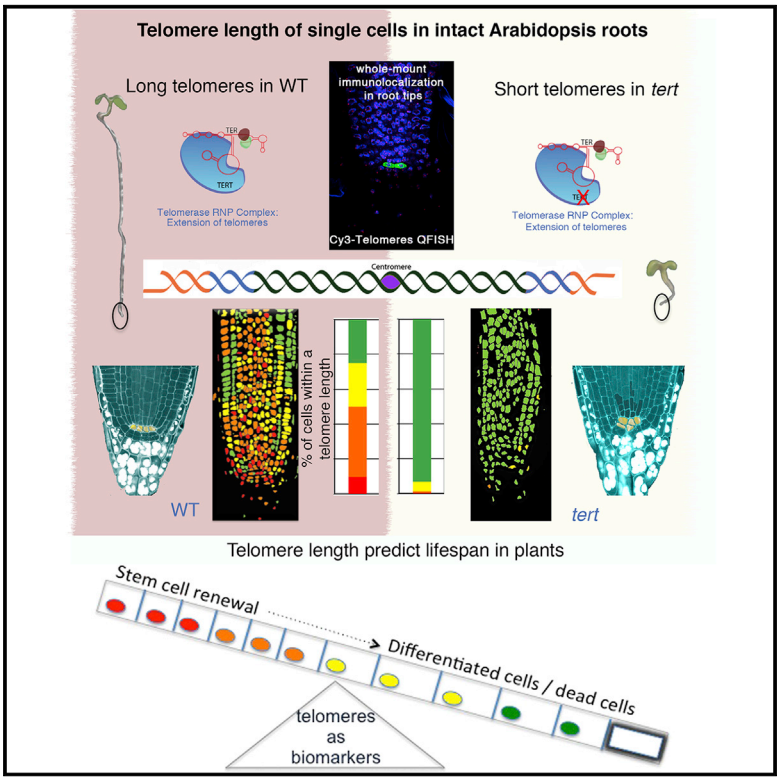

Highlights

- Heterogeneous telomere-length distribution in different root cell lineages
- Postembryonic telomerase activity is required for stem cell function in roots
- Telomerase sustains cell division at the meristem
- Premature cell differentiation can prevent telomere erosion in roots

Authors

Mary-Paz González-García, Irina Pavelescu, ..., Maria A. Blasco, Ana I. Caño-Delgado

Correspondence

ana.cano@cragenomica.es

In Brief

González-García et al. establish a Q-FISH methodology able to assess telomere length in individual cells at the *Arabidopsis* root apex, providing the first telomere-length distribution map in plants. The study reveals that telomere length is critical for meristem activity and stem cell renewal, thus coupling telomere dynamics to plant development.

González-García et al., 2015, Cell Reports *11*, 977–989
May 12, 2015 ©2015 The Authors
http://dx.doi.org/10.1016/j.celrep.2015.04.013

Cell Reports
Resource

Single-Cell Telomere-Length Quantification Couples Telomere Length to Meristem Activity and Stem Cell Development in *Arabidopsis*

Mary-Paz González-García,[1,6] Irina Pavelescu,[1,5] Andrés Canela,[2] Xavier Sevillano,[3] Katherine A. Leehy,[4,7] Andrew D.L. Nelson,[4,8] Marta Ibañes,[5] Dorothy E. Shippen,[4] Maria A. Blasco,[2] and Ana I. Caño-Delgado[1,*]
[1]Department of Molecular Genetics, Centre for Research in Agricultural Genomics (CRAG) CSIC-IRTA-UAB-UB, Barcelona 08193, Spain
[2]Telomeres and Telomerase Group, Molecular Oncology Program, Spanish National Cancer Centre (CNIO), Madrid 28029, Spain
[3]Grup de Recerca en Tecnologies Mèdia, La Salle - Universitat Ramon Llull, Barcelona 08022, Spain
[4]Department of Biochemistry and Biophysics, Texas A&M University, College Station, TX 77843, USA
[5]Department of Structure and Constituents of Matter, Faculty of Physics, University of Barcelona, Barcelona 08024, Spain
[6]Centro Nacional de Biotecnología (CSIC), Cantoblanco, 28049 Madrid, Spain
[7]Present Address: Departments of Medicine and Pharmacology, Masonic Cancer Center, University of Minnesota, Minneapolis, MN 55455, USA
[8]Present address: School of Plant Sciences, University of Arizona, Tucson, AZ 85721, USA
*Correspondence: ana.cano@cragenomica.es
http://dx.doi.org/10.1016/j.celrep.2015.04.013

SUMMARY

Telomeres are specialized nucleoprotein caps that protect chromosome ends assuring cell division. Single-cell telomere quantification in animals established a critical role for telomerase in stem cells, yet, in plants, telomere-length quantification has been reported only at the organ level. Here, a quantitative analysis of telomere length of single cells in *Arabidopsis* root apex uncovered a heterogeneous telomere-length distribution of different cell lineages showing the longest telomeres at the stem cells. The defects in meristem and stem cell renewal observed in *tert* mutants demonstrate that telomere lengthening by TERT sets a replicative limit in the root meristem. Conversely, the long telomeres of the columella cells and the premature stem cell differentiation *plt1,2* mutants suggest that differentiation can prevent telomere erosion. Overall, our results indicate that telomere dynamics are coupled to meristem activity and continuous growth, disclosing a critical association between telomere length, stem cell function, and the extended lifespan of plants.

INTRODUCTION

Telomeres are nucleoprotein structures at chromosome ends that allow proper chromosome segregation and are essential to maintain genomic stability. Since their original discovery in maize (*Zea mays*) (Sax and Enzmann, 1939), telomeres have become a central focus in the study of cancer, aging, and stem cell biology in mammals. Telomeres are maintained by telomerase, a ribonucleoprotein reverse transcriptase that employs a catalytic subunit TERT to reiteratively synthesize telomeric DNA on chromosome ends. Telomerase compensates for the inability of conventional DNA polymerases to replicate the ends of linear chromosomes and thereby circumvents the erosion of telomere tracts that naturally occurs with successive rounds of cell division (Lingner et al., 1995). The study of telomerase in mice demonstrated a rate-limiting role for telomerase in longevity and regeneration capacity due to stem cell dysfunction (Blasco et al., 1997b; Flores et al., 2005), and increasing telomerase levels can enhance the regenerative capacity of cells and increase both lifespan and health span (Bernardes de Jesus et al., 2012; Tomás-Loba et al., 2008).

Telomeric chromatin for most angiosperms consist of tandem repeats of the TTTAGGG DNA sequence bound by a set of telomere binding proteins that protect the chromosome ends and that have a high structural and functional similarity with their homologs in animals (Shakirov et al., 2010; Song et al., 2008; Surovtseva et al., 2009). As in animals, *Arabidopsis* tightly regulates telomerase expression and enzyme activity is confined to dividing tissues/organs (Watson and Riha, 2010). The absence of telomerase activity in mutants lacking *TERT* causes progressive telomere shortening and aberrant shoot development (Riha et al., 2001) arguing that telomere maintenance is essential for plant viability. However, the contributions of telomerase to most fundamental aspects of plant growth and development are largely unexplored.

Conventional molecular methods are available in *Arabidopsis* to assess bulk telomere length and the length of telomeres on individual chromosome arms using whole plants/organs (Heacock et al., 2004), yet the precise quantification of individual telomeres within a tissue or specific organ has not been examined. These techniques established that the average telomere length ranges between 2 and 5 kb in the Columbia ecotype (Richards and Ausubel, 1988; Shakirov and Shippen, 2004), and further that telomeres must exceed a critical length threshold of approximately 1 kb for genome stability (Heacock et al., 2004).

Based on the idea that telomeres progressively shorten with successive divisions in cells lacking telomerase, confocal telomere quantitative-fluorescence in situ hybridization (Q-FISH)

has been employed in animal models to trace the proliferative history of tissues and thus define the position of stem cell compartments (Flores et al., 2008; Jung et al., 2011; Martens et al., 1998). Although confocal telomere Q-FISH has provided a means of measuring telomere-length distribution along a given tissue section in animals, the *Arabidopsis* primary root is a superior system for imaging development in an intact organ. Its thin roots (~150 μm) can be captured within a single confocal stack of images, with low autofluorescence. Both characteristics allow in vivo nuclear imaging of an intact organ. In the roots, the meristem divisions of the different root lineages can be traced back to the position of the stem cells, thus offering an excellent system to trace cell division history in plant organs. The stem cell niche is formed by a small group (3–7) of slowly dividing cells that form quiescent center (QC) cells surrounded by the stem cell initials (Petricka et al., 2012; Scheres et al., 2002).

For these reasons, the primary root of *Arabidopsis* was chosen in this study to establish a high-throughput methodology able to assess the length of individual telomeres. Our analysis in the cells of the intact *Arabidopsis* root apex defines a telomere distribution map uncovering the existence of telomere gradients within plant cell types and demonstrates that telomere length is tightly coupled to meristem activity. Interestingly, these results explain the dramatically reduced stem cell renewal of *tert* roots, further substantiating the importance of telomere length in preserving the potential for cell division of plant stem cells. Collectively, our data demonstrated that telomere length assures the continuous stem cell renewal during root growth in plants.

RESULTS

Telomere Q-FISH Analysis in Intact Roots Enables the Quantification of Telomere Length with Tissue Resolution

Quantification of telomere length in plants has been reported using bulk tissue and organs by conventional molecular biology techniques (Fajkus et al., 1998; Riha et al., 1998), yet telomere length distribution within a plant organ has not been previously reported. In this study, we set up a whole-mount telomere Q-FISH-based (quantitative fluorescence in situ hybridization) method to quantify telomere fluorescence intensity in an intact organ with tissue resolution based on Flores et al. (2008). We used *Arabidopsis* root to capture confocal z stack of images within an intact organ and to quantify the telomere length of different cell layers along the longitudinal root apex (Figures 1A and 1B). This approach enables the analysis of single cells and preserves the structure of the cells (Figure S1; Movie S1).

As individual z-planes do not enable the visualization of all centromeres/telomeres present in the nuclei, the fluorescence intensity values were normalized with the number of fluorescence spots by dividing the sum of the intensities of all the individual centromeres/telomeres observable in a given cell, by their number. The averaged spots intensity value per cell was shown to avoid the detection of changes in fluorescence caused by ploidy, and/or nuclear size (see Supplemental Information). Furthermore, a 3D model for individual cells at the root apex was built from the stack of confocal images. A semi-supervised 3D segmentation process was conducted to create a three-dimensional model of the cell in which the centromeres/telomeres detected in the layer-wise quantization process were represented by red spheres. The diameter of these spheres is proportional to the measured size of the fluorescence spots. Moreover, the cell nucleus boundaries are used to build a 3D mesh that constitutes a faithful virtual reconstruction of the cell nucleus (Figure S1; Movie S2).

Initially, whole-mounted immunofluorescence using cell-specific GFP markers was used to visualize the position of specific cell types in the root under a confocal microscope. To mark the quiescence center (QC) or the bona fide stem cells, which are located at the median longitudinal plane of the root apex, we used the *WUSCHEL-related homeobox 5 pWOX5:GFP* (Figures 1C and 1D, rendered in green) (Sarkar et al., 2007). Subsequently, we performed quantitative FISH with a plant-specific telomere fluorescent peptide nucleic acid (PNA) probe (Cy3-[CCCAGGG]) to visualize and quantify individual telomere fluorescence signals at a cell level in the *Arabidopsis* root (Figure 1E). A merged image of GFP, Cy3, and DAPI channels enabled the visualization of telomeres inside individual nuclei of the root apex (Figures 1D–1G). The GFP labeling of QC allowed the precise identification of the stem cell compartment (Figure 1H; Movie S1). In the confocal Z-scan at the median longitudinal plane, DAPI-staining of the nuclei was used for nuclear area segmentation and binary mask generation (Figure 1I; Supplemental Information). Finally, the fluorescence quantification of individual telomere spots inside each nucleus in the confocal Z-scan was achieved by merging the binary mask with the Cy-3-labeled confocal image and using the Granularity module of the Metamorph platform (Supplemental Information). Collectively, this method allows the precise quantification of telomere length in an intact plant organ with cellular resolution.

A Telomere-Length Distribution Map for the *Arabidopsis* Primary Root Apex

The combination of immunofluorescence and telomere Q-FISH with quantitative imaging technology revealed a telomere-length distribution map for the *Arabidopsis* root apex (n = 2,541 nuclei) (Figure 2A). We found telomere-length heterogeneity between the different cells in the root meristem, suggesting that telomere length may be coupled to specific cells or cellular activities. The same pattern was observed among all individuals tested in our study (see Experimental Procedures; Figure S2). The fluorescence values representing individual telomere length per cell were quantified and plotted into frequency histograms and percentiles were calculated (Figures 2B and 2I; Supplemental Information). The value for the average telomere fluorescent intensity calculated was 636 ± 7 arbitrary units of fluorescence (a.u.f.), with 8% of the cells being significantly longer than their counterparts in the wild-type (WT) root (Figures 2A, 2B, and 2I). Next, we used *Arabidopsis tert* mutants to validate the ability of this technology to detect changes in telomere length. To this end, successive generations of *Arabidopsis tert* mutants (generations 3–5 [G3–G5] [Riha et al. 2001]) were subjected to the telomere Q-FISH analysis. The significant telomere shortening observed in successive generation of *tert* mutants (Figures 2C–2I; $p < 0.005$) further validates the sensitivity of the telomere Q-FISH method in the root. The reduction in the average telomere length

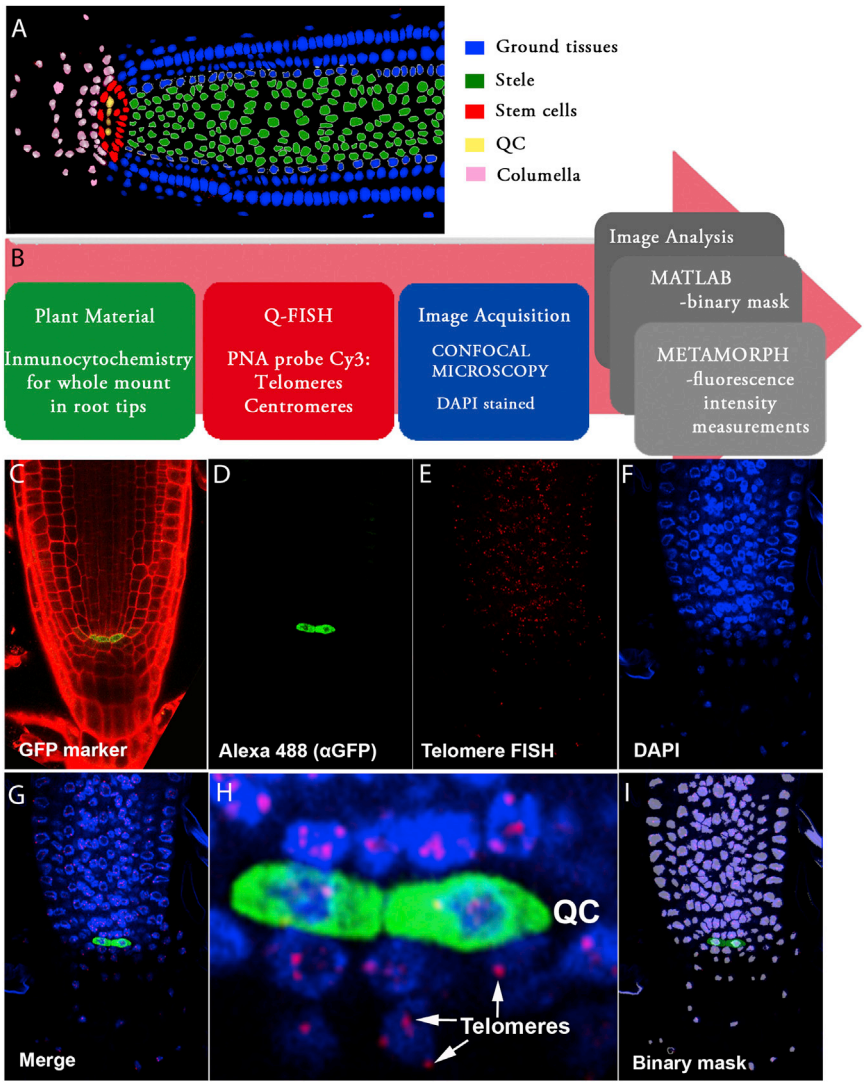

Figure 1. A Q-FISH-Based Telomere Distribution Map in the *Arabidopsis* Root Apex

(A) Schematic representation of meristem organization in a 6-day-old *Arabidopsis* root. The color code identifies the different cell types: ground tissues (epidermis, cortex, endodermis, and lateral root cap) in blue, stele in green, stem cell niche in red, quiescent center (QC) in yellow, and columella cells in pink.

(B) Pipeline describing the experimental setup for whole-mount root telomere Q-FISH. Six-day-old *Arabidopsis* roots were subjected to a whole immunocytochemistry process using GFP markers (green box). GFP immunofluorescence was combined with confocal Q-FISH directly using a PNA Cy3-labeled telomeric/centromeric probe (red box). DAPI, Cy3, and Alexa 488 signals were acquired simultaneously into separate channels using a confocal microscope. The DAPI image was used to define the nuclear area to create a binary mask that allows isolation of each nucleus (blue box). The segmentation method was implemented using MATLAB (gray box). In the final step of the pipeline, Metamorph software was used to combine the binary DAPI mask and the matching Cy3 image. Cy3 fluorescence intensity (telomere fluorescence) was measured as "average gray values" units (a.u. of fluorescence). A code of four colors was used to classify the nuclei according to their average telomere fluorescence (gray box). A large pink arrow indicates the flow direction of the whole mount root Q-FISH procedure.

(C) Six-day-old roots stained with PI. The GFP marker (green) stains the *pWOX5:GFP* expression domain, coinciding with the quiescent cells.

(D–G) Confocal images showing the QC labeled by *pWOX5:GFP* (D), Q-FISH using a telomeric PNA probe stained with Cy3 (E), cell nuclei stained with DAPI (F), and a merged image for all three channels (G).

(H) Inset showing, with cellular resolution, the QC and surrounding cells, together with their corresponding telomeres indicated by arrows.

(I) Binary mask generated in MATLAB and used for individual nuclei fluorescence intensity quantification (see the Supplemental Information).

in the root apex of G3 *tert* (524 ± 7 a.u.f.; Figures 2C and 2D) and G4 *tert* (475 ± 9 a.u.f.; Figures 2E and 2F) was even more dramatic in the roots of G5 *tert* (250 ± 8 a.u.f.; Figures 2G and 2H) compared to WT plants (636 ± 7 a.u.f.; Figures 2A, 2B, and 2I; Figure S2).

Notably, telomere-length heterogeneity was lost in later-generation *tert* mutants, pointing to eventual exhaustion of telomere signals owing to the prolonged absence of telomerase activity (Figure 2I). Notably, in G5 *tert* roots a very small fraction of cells (1%) had telomeres longer than the rest of the cells in the root apex (Figure 2I; represented in red). This phenotype was even more dramatic in G6 *tert* roots (Figure S3).

Next, we validated the differences in telomere length observed using telomere Q-FISH in *tert* mutants by performing an independent technique based on qPCR. To this end, we used primer extension telomere repeat amplification (PETRA), which allows for the quantification of telomere length of individual chromosome arms (Heacock et al., 2004) in bulk tissues. PETRA was performed on DNA extracted from root tips to measure the telomere length for the right arm of chromosomes 2 (2R) and 5 (5R) and the left arm of chromosome 3 (3L). PETRA products confirmed telomere shortening in roots from successive generations of plants lacking TERT (Figures 2J and 2K). As the fluorescence intensity resulting from telomere Q-FISH is directly proportional to the telomere length (Vera and Blasco, 2012), we used PETRA values to convert a.u.f. values into kilobases. To this end, we plotted average telomere fluorescence values against the sizes of PETRA fragments in WT and G3–G5 *tert* mutants. Linear regression analysis estimated that 1 kb corresponds to 215 a.u.f. (Figure S2). We observed that the telomeric distributions were not normal, with positive skewness and with minimal values above 75 a.u.f. This cutoff might be due to an optimal telomere length value required for the normal functioning of the cell and not by our method, since our technique

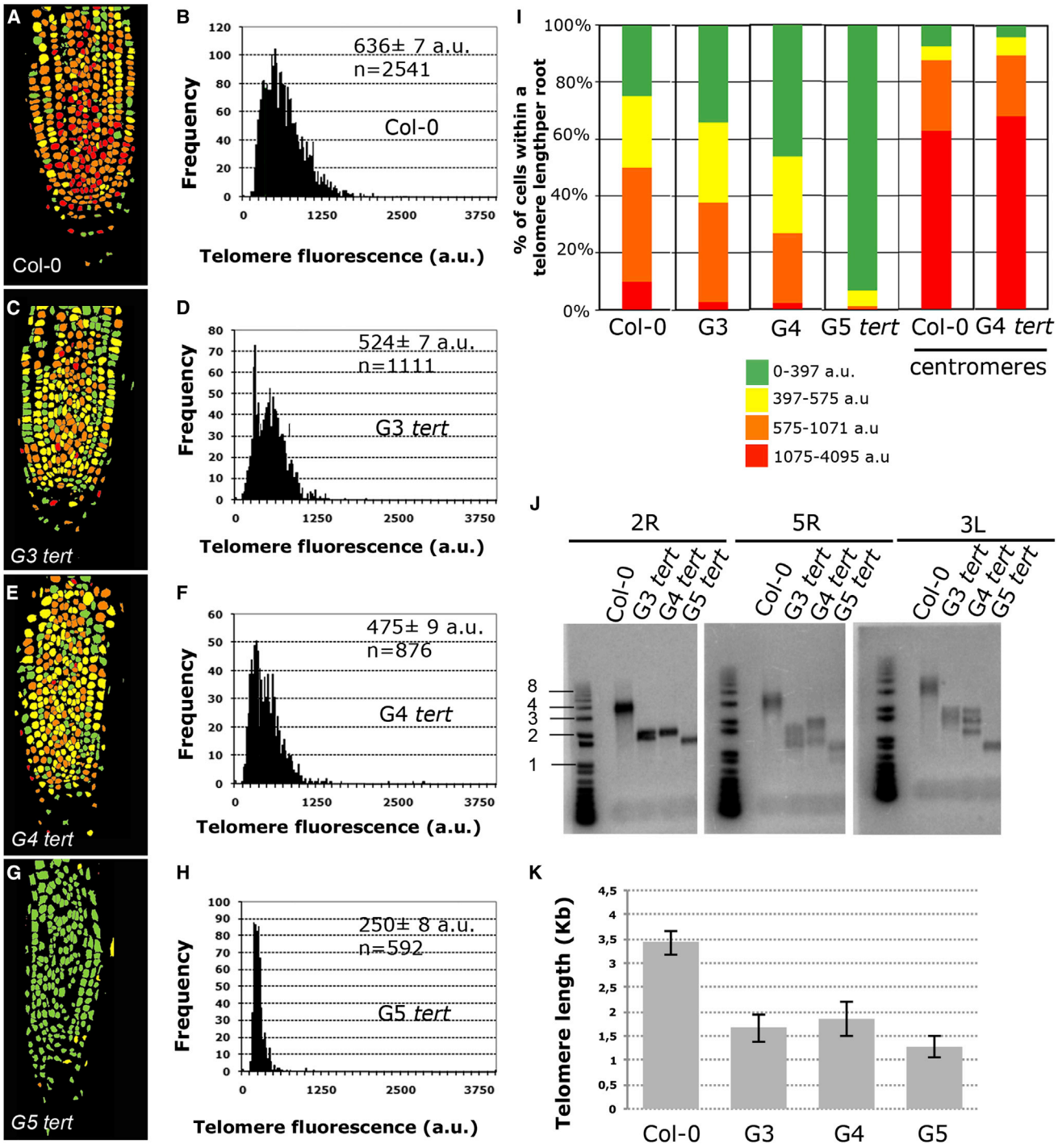

Figure 2. Telomere-Length Analysis by Whole-Mount Root Q-FISH of Successive *tert* Mutant Generations

(A, C, E, and G) Representative telomere-length pseudo-color images in 6-day-old roots of WT (A), G3 *tert* (C), G4 *tert* (E), and G5 *tert* (G).

(B, D, F, and H) Telomere Q-FISH histograms showing telomere fluorescence frequencies in WT (B), G3 *tert* (D), G4 *tert* (F), and G5 *tert* plants (H). Average telomere fluorescence and SEM are indicated. See also Figure S2.

(I) Percentage of cells showing a given telomere fluorescence in WT, G3 *tert*, G4 *tert,* and G5 *tert* and centromere fluorescence in WT and G4 *tert* plants. Note the significant enrichment in cells with short telomeres in *tert* mutants (green color) and also the lack of changes in centromere fluorescence (see also Figures S1 and S2).

(J) PETRA analysis of telomeres on 2R, 5R and 3L chromosome arms in WT and (G3–G5) *tert* mutant generations. A telomeric probe was used to detect PETRA products (see Experimental Procedures). See also Figure S2.

(K) Quantification of the average telomere length in Kb of PETRA bands of different chromosome arms of DNA extracted from roots of WT and (G3–G5) *tert* plants. The data shown in (B), (D), (F), (H), and (I) were collected by pooling seven individuals plants of WT Col-0, three G3 *tert*, three G4 *tert*, and three G5 *tert*.

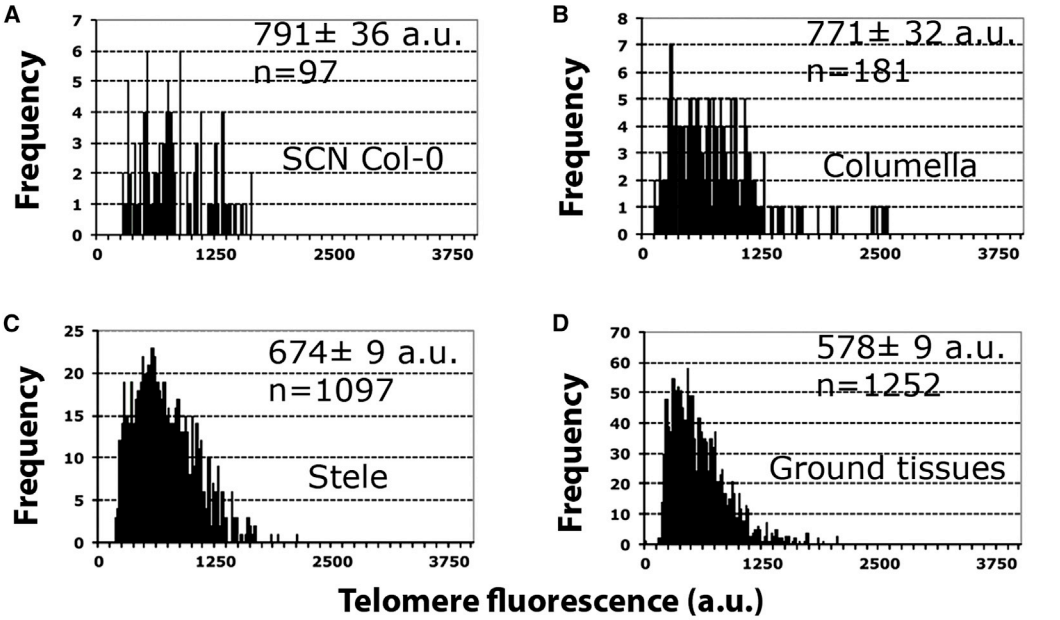

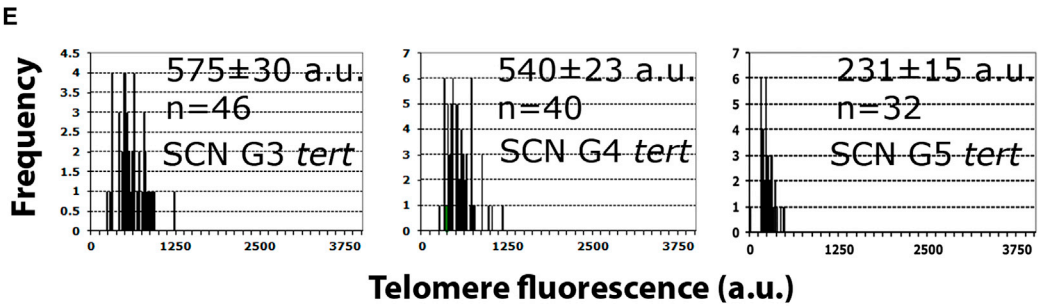

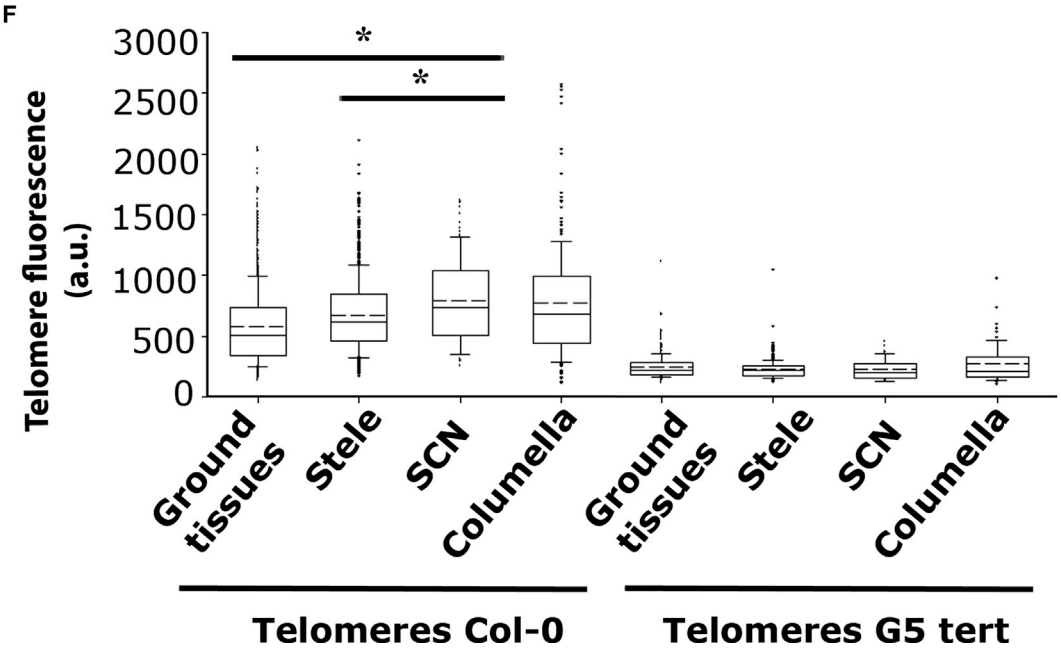

(legend on next page)

is sensitive enough to detect telomeres in G6 *tert* mutants that were shown to be extremely short by PETRA experiments (Figure S3).

Finally, to verify that the observed differences in telomere length did not reflect changes in probe accessibility, a PNA probe specific for the *Arabidopsis* centromere repeat sequence (Cy3-GACTCCAAAACACTAACC) was applied following the same methodology (Experimental Procedures; Supplemental Information). Centromere fluorescence intensity of WT and G4 *tert* roots was quantified (Figure 2I). The average fluorescence intensity of WT plants (1,274 ± 17 a.u.f.; n = 1,088 nuclei) was compared to G3 *tert* (1,601 ± 26 a.u.f.; n = 693 nuclei) and to G4 *tert* (1,305 ± 19 a.u.f.; n = 753 nuclei; Figure S1). The absence of significant changes in centromere intensity between the different generations of root cells confirms that the observed changes in telomere intensity are not caused by differences in the hybridization procedure but instead reflects progressive telomere shortening owing to telomerase deficiency. Furthermore, our data reveal that TERT maintains heterogeneous telomere length distribution within the root apex.

Cells within the Stem Cell Compartment Display the Longest Telomeres

To further investigate the origin of the telomere length variability observed in WT primary root and to check whether it can be attributed to specific cellular activities, we measured the telomere length in different root cell types.

The *Arabidopsis* root system offers a set of specific cell-type markers based on promoter-GFP fusions that can be used to trace the location of different root cell types (Figure S4). Using these markers, we analyzed the telomere length in the outer cell layers (ground tissues), the stele (inner cells layers), the stem cell niche (SCN), and the columella cells (Figure 1A). Interestingly, the cells with the longest telomeres were enriched at the position of the known SCN (791 ± 36 a.u.f.; $p < 0.05$) (Figure 3A), although no significant differences in telomere length could be detected between the QC and the surrounding stem cells (Figure S2). The telomere length of the SCN was undistinguishable from that of the columella cells (771 ± 32 a.u.f.), which differentiated after a single columella stem cell division (Scheres et al., 2002; Figure 3B). Telomere length was significantly shorter in the stele (674 ± 9 a.u.f., $p < 0.05$) (Figure 3C) and the ground tissues (578 ± 9 a.u.f., $p < 0.05$) (Figure 3D). Next, we analyzed the stem cell niche telomere-length distributions for G3–G5 *tert* mutants, which appeared increasingly shorter than those of the corresponding WT controls (Figure 3E; $p < 0.001$). Remarkably, no differences in average telomere length were observed for the different cell types of G5 and G6 *tert* mutants, consistent with the loss of heterogeneity shown in the *tert* mutant heatmap (Figure 3F; Figure S3).

These differences in telomere length between different cell populations within the *Arabidopsis* root suggest the use of whole-mount telomere Q-FISH as a powerful method to visualize telomere length distribution in the *Arabidopsis* roots that can be associated with specific cells and/or cellular activities, such as telomerase activity. The lack of differences in telomere length between SCN and columella cells suggests that telomere length correlates to the number of cell division prior differentiation.

Telomerase Sustain Cell Division at the Root Meristem

Previous studies showed that telomerase activity is present in rapidly dividing plant cells but undetectable in differentiated tissues (Fitzgerald et al., 1996, 1999). Here, we sought to investigate the functional consequences of critical telomere shortening owing to telomerase deficiency in the potency of meristematic cells in *Arabidopsis*. We first confirmed abrogation of telomerase activity in the *tert*-deficient *Arabidopsis* roots by using the TRAP (telomere repeat amplification protocol) assay. As expected, the root tips of 6-day-old WT seedlings exhibited telomerase activity, which was undetectable in G4 *tert* mutants (Figure S5). To test whether TERT is required post-embryonically to restore telomere shortening associated with divisions during the primary root growth, we analyzed meristem development in roots from *tert* mutants (Figures 4A–4D). Concomitant with the loss of telomerase activity, successive generations of *tert* (G4–G6) exhibited a progressive reduction of root growth and meristem size compared to WT (Figures 4B and 4D). Next, we studied the expression of D-box *pCYCB1;1:GFP* reporter (González-Garcia et al., 2011; Ubeda-Tomás et al., 2009), which marks proliferating cells, and performed immunostaining using the cytokinesis-specific syntaxin KNOLLE (Völker et al., 2001) in WT and increasing generation of *tert* mutant roots. We observed that *tert*-deficient roots showed a reduction in the number of mitotically active cells, as marked by *pCYCB1;1:GFP* (Figures 4J and 4L) as well as in the number of cell plates labeled by anti-KNOLLE antibodies (Figures 4H and 4K) with increasing plant generations in contrast to WT (Figures 4G and 4I). Furthermore, late-generation *tert* mutants displayed increased levels of the plant-specific cell-cycle inhibitor *pICK2/KRP2:GUS* (De Veylder et al., 2001) as compared to the WT (Figures 4E and 4F). To further confirm a relationship between telomere length and meristem activity, we studied roots with null mutation in *KU70*, a negative regulator of telomere length, and thus

Figure 3. The Longest Root Telomeres Are Mapped in the Stem Cell Niche

(A–D) Q-FISH histogram showing telomere fluorescence frequencies in the different cell types of Col-0 root: stem cell niche (SCN) (A), columella (B), stele (C), and ground tissues (D). Average telomere fluorescence and SEM are indicated. See also Figure S2.

(E) Q-FISH histograms of G3, G4, G5 *tert* stem cell niche. Note the high difference in telomere length compared to Col-0 stem cell niche.

(F) Boxplots showing the heterogeneity between cell types in telomere-length distributions of Col-0 compared to G5 *tert*. Boxes represent the interquartile range (25^{th}–75^{th} percentiles, median indicated by the black horizontal line, average indicated by the dashed line) of the distribution, whiskers extend to the 10^{th} and 90^{th} percentiles and outliers are represented by black dots. n represents the number of nuclei pooled for the histograms from seven individual Col-0 plants and from three plants for each G3, G4, and G5 *tert* mutants. For Col-0 and G5 *tert* roots, SCN telomere-length values were compared to ground tissues, stele, and columella values. Statistical significant differences were observed in Col-0 only between SCN and stele and between SCN and ground tissues. In the G5 *tert* mutants, no differences were observed between cell types. *$p < 0.05$.

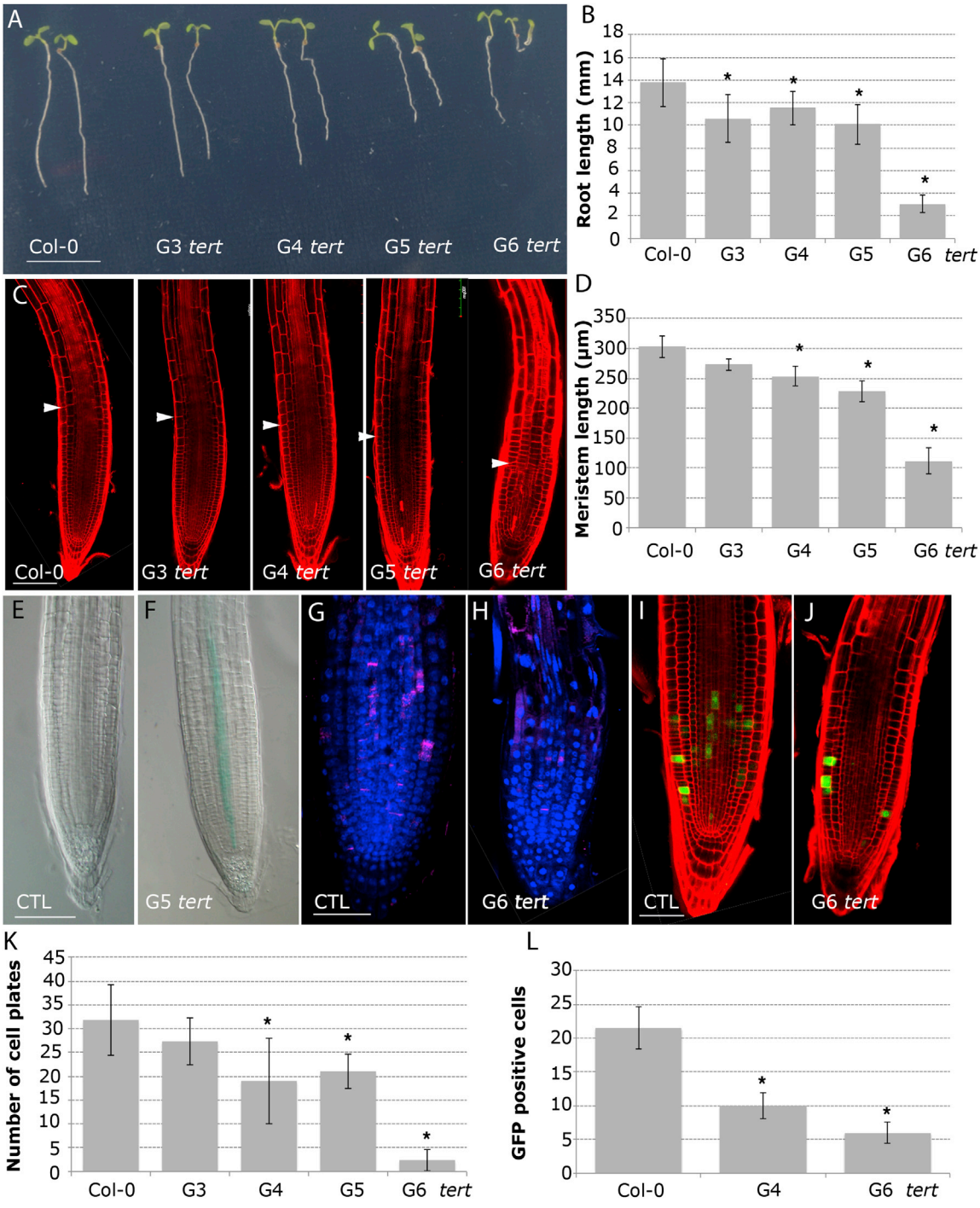

Figure 4. Active Telomerase Is a Requirement to Preserve Cell Division during Root Growth

(A) Morphology of 6-day-old seedlings of WT and (G3–G6) *tert* plants. Scale bar, 10 mm. (See also Figure S3.)

(B) Root-length measurements of (G3–G6) *tert* seedlings compared to the WT. Asterisks denote a statistically significant difference with WT ($p < 0.005$).

(C) Confocal images of 6-day-old WT and (G3–G6) *tert* roots stained with PI. Arrows mark the boundary between the proximal meristem and the elongation zone of the root. Scale bars, 100 µm.

(D) The meristem length of 6-day-old roots of (G3–G6) *tert* mutant generations compared to WT. Asterisks indicate significant differences relative to WT for each day ($p < 0.005$).

(E and F) GUS staining of 6-day-old roots expressing *pICK2/KRP2:GUS* (E) and G5 *tert*; *pICK2/KRP2:GUS* (F). Scale bar, 50 µm.

(G and H) Whole-mount immunofluorescence using anti-KNOLLE antibodies in WT (G) and G6 *tert* (H). Scale bar, 50 µm.

(legend continued on next page)

presenting longer telomeres than WT plants (Riha et al., 2002). Interestingly, we found that KU70 deficiency leads to both longer telomeres and increased meristem size relative to WT roots (Figure S3, $p < 0.005$). Together, these results indicate that telomere length is linked to meristem potency in plants.

Telomere Length Sets a Replicative Limit in the Stem Cells

Our observations showing that cells with the longest telomeres are enriched at the root stem cell compartment (Figure 3) together with the loss of meristem activity of *tert* mutants (Figure 4) prompted us to investigate the impact of telomere length on plant stem cell function. Microscopic analysis of roots revealed that, relative to WT, *tert* mutants displayed striking differences in the anatomy of the stem cell niche. We observed an increased cell division rates in the QC of *tert* mutants (Figures 5A–5G). In particular, the majority of G6 *tert* plants (86%) had additional QC divisions while only 7% of WT plants showed this phenotype (Figure 5J). Concomitantly, confocal images of modified pseudo-Schiff (mPS)-PI-stained roots revealed the presence of starch granules in former columella stem cells, indicative of increased stem cell differentiation dynamics in *tert* mutants (Figures 5B–5E and 5K), whereas in the WT starch granules were normally absent from columella stem cells (Figures 5A and 5K). Consistent with these phenotypic defects at the stem cell niche, *tert* mutants exhibited an altered expression of QC-specific marker *pWOX5:GFP* (Sarkar et al., 2007) (Figures 5F and 5G) and the death of stem cells (Figures 5H and 5I). The cell death phenotype worsened in late *tert* generations so that propidium iodide (PI) staining was present in 100% of G6 *tert* mutants analyzed (Figure 5L).

Similar to what has been described for mammals (d'Adda di Fagagna et al., 2003; Herbig et al., 2004), plant telomere dysfunction generates a DNA-damage response (DDR) that activates ATM/ATR kinase pathways and results in programmed cell death (PCD) (Boltz et al., 2012). To assess early DDR responses dependent on ATM/ATR kinases, we analyzed the phosphorylation of γ-H2AX (Amiard et al., 2011). Confocal immunofluorescence using γ-H2AX antibodies in G6 *tert* roots revealed the presence of γ-H2AX-labeled foci co-localizing with telomeres (the so-called TIFs or telomere-damage-induced foci) in the majority of living cells at the G6 *tert* mutants root meristem (Figures 5O and 5P and inset in Figure 5Q) compared to the WT controls where the labeling with γ-H2AX was undetectable (Figures 5M and 5N). These results show that telomerase preserves genomic stability by preventing critical telomere loss and the activation of DDR downstream signaling events that cause stem cell loss and meristem exhaustion.

Telomere Q-FISH Reveals Longer Telomeres in *plt1 plt2* Mutants

To further investigate whether cell differentiation can prevent telomere erosion and how telomere attrition affects the behavior of different stem cells in the root, we analyzed telomere length in *plt1 plt2* mutants (Aida et al., 2004). PLETHORA (PLT) transcription factors are central regulators of stem cell differentiation and meristem maintenance in the *Arabidopsis* root apex. Mutations in *PLT* cause premature stem cell differentiation, leading to the formation of dramatically shortened, aberrant roots (Figures 6A, 6B, and S6) in agreement with Aida et al. (2004) and Galinha et al. (2007). Strikingly, telomere Q-FISH analysis in whole-mounted roots of *plt1 plt2* revealed a significant increase ($p < 0.001$) in average telomere fluorescence (1,214 ± 32 a.u.f.; n = 324 nuclei; n = 3 roots; Figures 6G and 6H) compared to WT (Ws-2) plants (934 ± 14 a.u.f.; n = 1,152 nuclei; n = 3 roots; Figures 6E and 6F). These results were confirmed molecularly by TRF (Figure 6C) and PETRA assays (Figure 6D). The increase in telomere length in *plt1 plt2* plants relative to WT can be explained by the reduced replicative history of *plt1 plt2* cells before they undergo differentiation (Aida et al., 2004).

DISCUSSION

The plant meristem sustains the production of cells through an organismal lifespan that reaches thousands of years in some plant species. Whether telomeres contribute to the replicative senescence in plants has been subject of a long-standing controversy (Gan, 2003; Watson and Riha, 2011). In this study, we integrated genetic, cellular, and molecular tools to dissect the contribution of telomere maintenance to plant stem cell renewal. We first describe here that, similar to that found within the normal architecture of mammalian tissues (Flores et al., 2008; Vera and Blasco, 2012), telomere length is not uniformly distributed among root cell types in the meristem of *Arabidopsis*. Instead, cells with the longest telomeres are enriched at the known stem cell compartments, and proper telomere maintenance in these compartments is essential for their ability to sustain meristem growth.

In animals, gradual telomere shortening in the absence of telomerase is proposed to act as mitotic clock that limits cell proliferation capacity (Harley et al., 1990). While such a mechanism is useful to inhibit rapid growth of tumors, telomere attrition in stem cells exhausts their proliferation capacity and contributes to organismal aging (Blasco et al., 1997a). In plants, telomerase activity is associated with all proliferative organs and is absent in fully differentiated tissues such as stem and leaves (Riha et al., 1998) suggesting that differential expression of telomerase influences plant development (Gan, 2003; Thomas, 2013). Our analysis documents that meristem activity and stem cell function are intimately connected to the ability of telomeres to maintain genomic stability in plants.

Here, we exploited the amenability of experimenting with *Arabidopsis* primary roots to address how telomere-length dynamics is coupled to plant meristem development. We found that telomerase activity is maintained post-embryonically in specific root cells in the root apex together with the preferential

(I and J) *pCYCB1;1:GFP* expression in WT roots (I) and G6 *tert* (J). Scale bar, 50 μm.
(K) Number of cell plates calculated in whole-mount immunofluorescence with anti-KNOLLE antibodies present in (G3–G6) *tert* seedlings compared to the WT.
(L) Number of GFP cells in the meristem of *pCYCB1;1:GFP* ($p < 0.001$) and G4 *tert* and G6 *tert* seedlings ($p < 0.001$). Asterisks denote a statistically significant difference with the WT ($p < 0.001$).

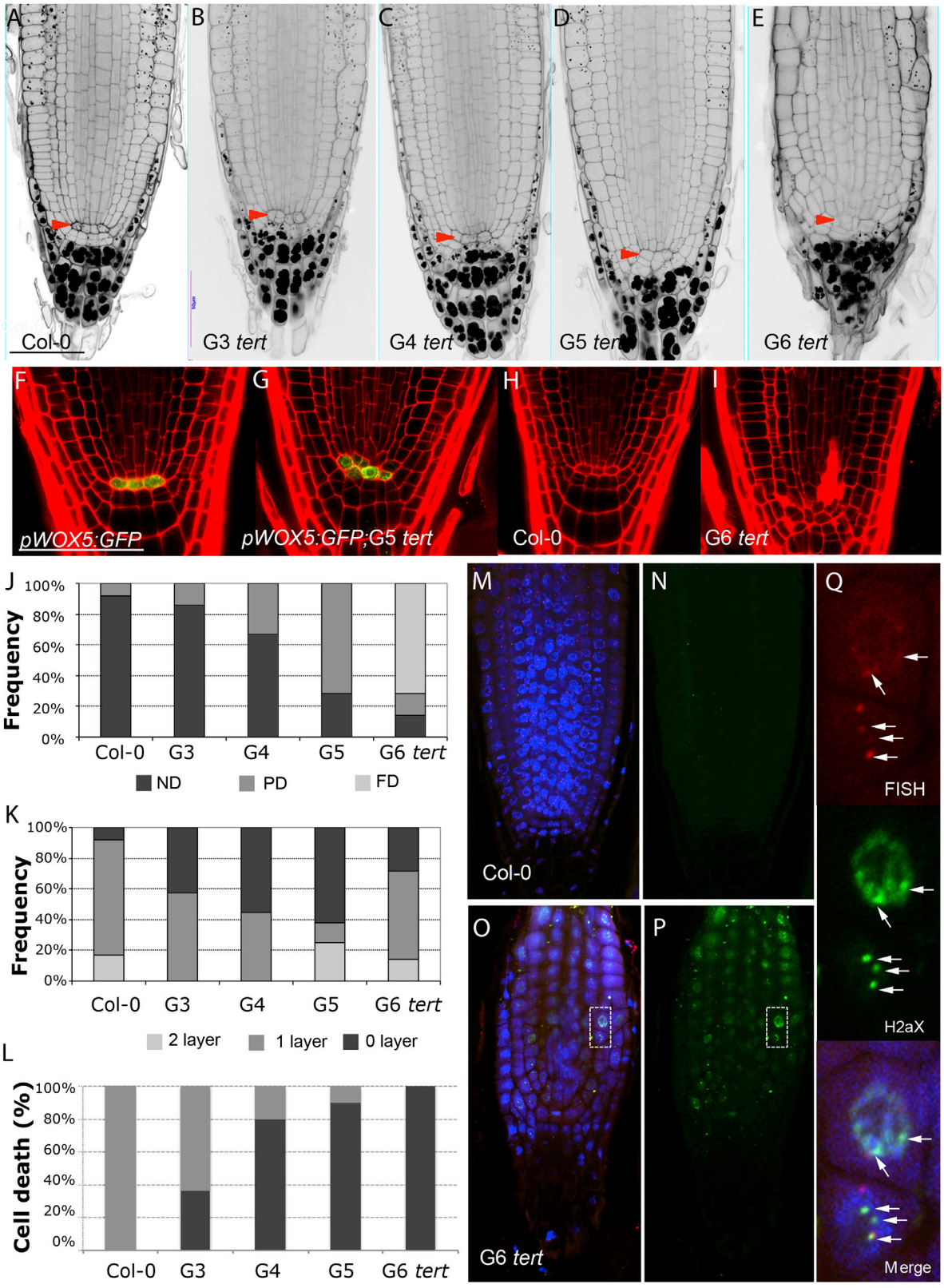

(legend on next page)

transcription of TERT mRNA in specific cells at the meristem (Brady et al., 2007) supporting a role for telomerase in maintenance of meristem growth. In the root, telomere length defines two important features of root growth and development: meristem division and stem cell replenishment. Both are essential to ensure the reproductive phase of development and lifespan in plants (Mencuccini et al., 2005). We found that telomere shortening in *Arabidopsis* roots causes cell-cycle arrest that is associated with phenotypic changes resulting in reduced root growth as shown by a marked reduction of meristem cell number, reduced mitotic activity, and the accumulation of the cell-cycle inhibitors ICK2/KRP2. These changes, together with the presence of telomere-localized γ-H2AX in the meristematic cells, support a model in which telomere length sets a replicative limit for a functional and living meristem in plants.

Additional evidence supporting the hypothesis that cell division can be recorded by telomere length in plants is provided by the longer telomeres in the roots of stem cell mutants *plt1 plt2*, which have undergone premature differentiation (Aida et al., 2004). While short telomeres limit cell divisions in the meristem, long telomeres cannot prevent cell differentiation as indicated by the increased telomere length in differentiated columella cells in WT and *plt1 plt2*. Rather *plt1 plt2* mutants maintain their regenerative potential when their root tips are excised (Galinha et al., 2007). Thus, preserving telomere length during the division of stele cells appears to be a critical mechanism controlling root growth and development.

Intriguingly, we found that short telomeres in late-generation *tert* mutant plants show an increased frequency of QC division. These unscheduled divisions resembled those of plants subjected to genotoxic stress consistent with known responses of the QC to DNA damage (Cruz-Ramírez et al., 2013; Vilarrasa-Blasi et al., 2014) and reflecting the need of telomerase to ensure stem cell renewal in plants. Moreover, in *tert* stem cells, the absence of telomeric γ-H2AX foci and the increase of cell-cycle inhibitors pICK2/KRP2 argue that critically short telomeres activate an irreversible DNA damage signal that not only promotes death but also increase susceptibility to DNA damage for stem cells relative to their descendants in the meristem (Fulcher and Sablowski, 2009). This proposition is consistent with current models for premature senescence of mammalian stem cells (López-Otín et al., 2013; Rossi et al., 2008), uncovering the potential of plants as a model for studying telomere length control of stem cell function in eukaryotes. Further analysis of telomere-length gradients can reveal new insights into developmental circuitry and functional stem cell pools, and also serve as a basis for mechanistic comparison of plant and animal regeneration and lifespan.

Finally, while there are no technical constrains that limit the quantification of telomeres by Q-FISH in additional plant species, this technology opens new possibilities for the study of meristem and stem cell function in other plant systems, especially in perennial species.

EXPERIMENTAL PROCEDURES

Plant Material and Microscopy

Arabidopsis thaliana (L.) Heyhn. seed accessions Columbia (Col-0), Wassilewskija (Ws-2), *plt1 plt2 mutants* (Aida et al., 2004; Galinha et al., 2007), *tert* mutants (Riha et al., 2001), *ku70* (Riha and Shippen, 2003), and all marker lines *pWOX5:GFP* (Sarkar et al., 2007), *pGL2:GFP* (Lin and Schiefelbein, 2001), *pSCR:GFP* (Sabatini et al., 1999), *pWOL:GFP* (Mähönen et al., 2000), QC12 (Lee et al., 2006), DR5:GFP (Ulmasov et al., 1997), *pARF7:ARF7-GFP* (Rademacher et al., 2011) were used in this study. Seeds were surface-sterilized in 35% sodium hypochlorite, vernalized 72 hr at 4°C in darkness, and grown on vertically oriented plates containing 1 × Murashige and Skoog (MS) salt mixture, 1% sucrose, and 0.8% agar. Plates were incubated at 22°C and 70% humidity under long-day conditions (16 hr light/8 hr dark).

A FV 1000 confocal microscope (Olympus) was used throughout the study. Roots were stained in 10 μg/ml propidium iodide (PI) for 2–5 min, rinsed, mounted in dH_20, and visualized after excitation by a Kr/Ar 488-nm laser line. PI and GFP were detected with a band-pass 570- to 670-nm filter and 500- to 545-nm filter, respectively. For the yellow and cyan fluorescent protein GFP-tag reporter, the excitation wavelengths were 488 nm fluorescence collected in the ranges of 493–536 nm (rendered in green). For every fluorochrome, image z stacks were taken with a sampling distance of 1 μm along the z axis and 200 μm in the x, y direction. To standardize the fluorescence between samples, the same exposure time was used for all Cy3 images. Starch granules in columella cells were visualized by a modified pseudo-Schiff (mPS)-PI staining method (Truernit et al., 2008).

Immunofluorescence and Q-FISH

Whole-mount immunolocalization in 6-day-old roots was performed as described (González-García et al., 2011) with minor modifications. Immunolocalization using anti-GFP and anti-KNOLLE antibodies was done as reported by González-García et al. (2011) and for γ-H2AX immunostaining antiserum diluted 1:600 using Alexa 488 as a secondary antibody in all cases (Amiard

Figure 5. Telomere-Length Gradients Control Stem Cell Function in the Root Apex

(A–E) mPS-PI-stained root tips of Col-0 (A) and G3 *tert* (B), G4 *tert* (C), G5 *tert* (D), and G6 *tert* (E) roots. Col-0 roots show normally one tier of columella stem cells (CSC). Red-arrow indicated QC cells.

(F and G) Confocal images of primary roots expressing *pWOX5:GFP* in the QC cells in WT (F) and G5 *tert* mutants (G).

(H and I) Cell death in the stem cells and adjacent daughter cells detected in WT (H) and G6 *tert* roots (I).

(J) Frequency distribution of QC division in (G3–G6) *tert* seedlings compared to the WT. PD, partially divided; ND, non-divided; FD, fully divided.

(K) Quantitative analysis of the effects of telomere length on CSC differentiation. Frequency distribution of the number of cell layers is given between the QC and the first differentiated columella cells that contain starch granules. Gradual differentiation of CSC in *tert* mutants is revealed by the frequency of roots without CSC layer.

(L) Cellular damage at the stem cells and vascular descendants was scored by counting intense PI-stained roots of WT and (G3–G6) *tert* plants.

(M and N) Immunostaining with γ-H2AX antibodies and telomere Q-FISH, cell nuclei stained with DAPI, telomeric PNA probe stained with Cy3, γ-H2AX foci colored in green, and a merged image for all the three channels of the WT.

(O and P) Immunostaining with γ-H2AX antibodies and telomere Q-FISH, cell nuclei stained with DAPI (blue), telomeric PNA probe stained with Cy3, γ-H2AX foci colored in green, and a merged image for all the three channels of the G6 *tert*. Note: for better visualization the laser intensity of the Cy3, channel was increased.

(Q) Inset shows magnification (dotted box) revealing the colocalization of γ-H2AX foci with the Cy3-telomere probe (white arrows). Due to the extremely short telomeres of G6 *tert* mutants, these images were captured by increasing the confocal laser power.

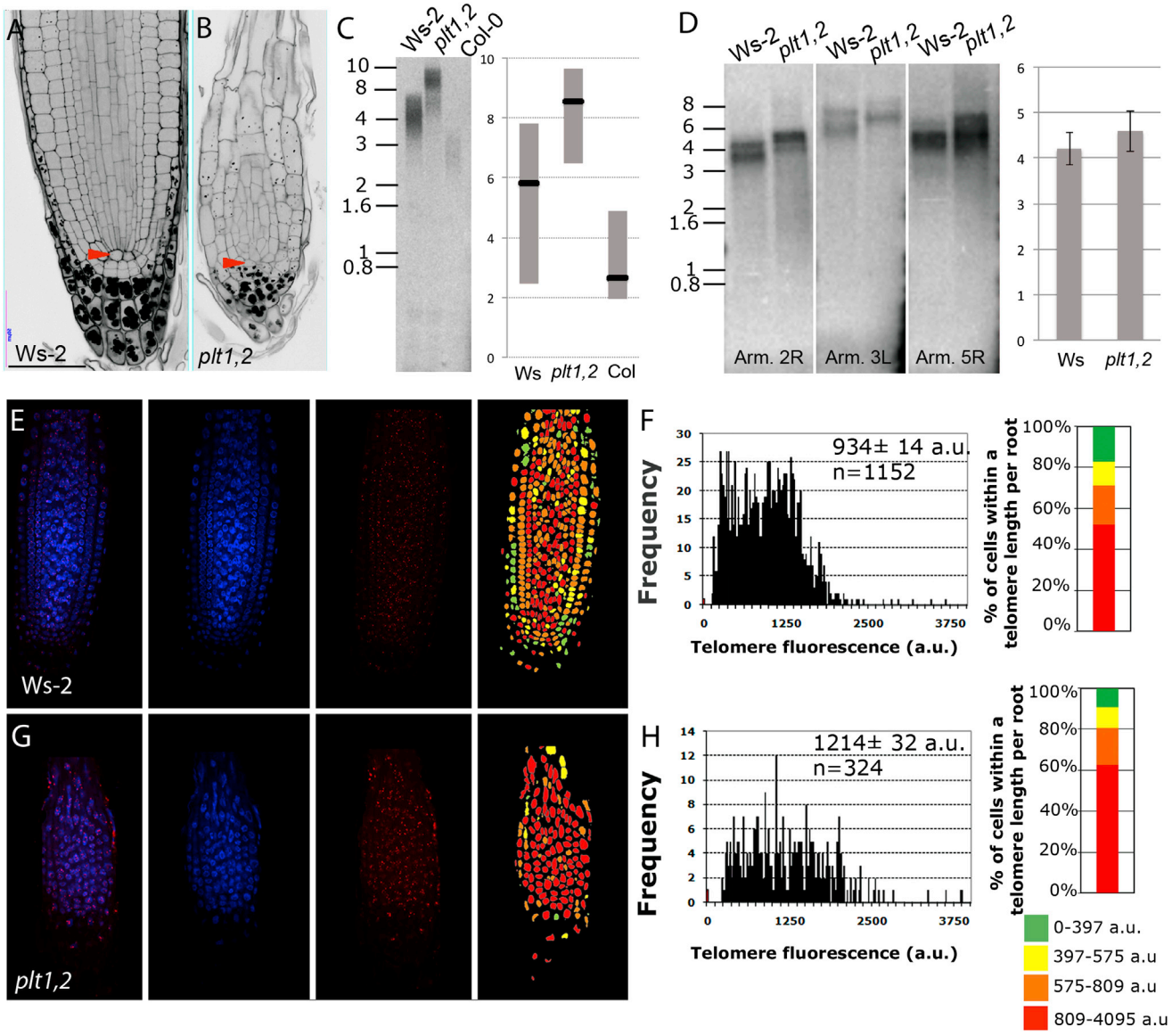

Figure 6. Early Differentiation in the Meristems of *plt1 plt2* Mutants Prevents Telomere Erosion in the Primary Root

(A and B) mPS-PI-stained root tips of 6-day-old WT (Ws-2) (A) and *plt1 plt2* (B) roots. Scale bars, 100 μm. See also Figure S6.

(C) TRF analysis in shoot of WT (Ws-2) and *plt1 plt2* mutants. The blot was hybridized with a radiolabeled telomeric (T3AG3)4 probe. Molecular weight markers and a schematic representation of the chromosome length are indicated.

(D) PETRA analysis of the 2R, 5R, and 3L telomeres in WT (Ws-2) and *plt1 plt2*. A telomeric probe was used to detect PETRA products. Molecular weight markers are indicated. Quantification of the average telomere length in kilobases of PETRA bands of different chromosome arms in WT (Ws-2) and *plt1 plt2*.

(E) Q-FISH in Ws-2 root telomeric PNA probe stained with Cy3, cell nuclei stained with DAPI, and a merged image for both channels. Representative telomere-length pseudo-color images of WT. Nuclei are colored according to their average telomere fluorescence in a.u.

(F) Q-FISH histogram showing telomere fluorescence frequencies in Ws-2. Average telomere fluorescence, SEM and the number of nuclei n, pooled from three individual Ws-2 plants, are indicated.

(G) Q-FISH in *plt1 plt2* root telomeric PNA probe stained with Cy3 cell nuclei stained with DAPI and a merged image for all the two channels. Representative telomere-length pseudocolor images of WT. Nuclei are colored according to their average telomere fluorescence in a.u. See also Figure S6.

(H) Q-FISH histogram showing telomere fluorescence frequencies in *plt1 plt2*. Average telomere fluorescence and SEM are indicated. Average telomere fluorescence, SEM, and the number of nuclei n, pooled from three individual *plt1 plt2* plants, are indicated.

et al., 2011). DAPI and Alexa 488 signals were acquired sequentially in two separated channels. Combined immunostaining with telomere Q-FISH was done to precisely mark by GFP the position of the stem cell niche in the whole-mounted roots. For Q-FISH, microscope slides were rinsed in 4% formaldehyde for 2′ and then washed with 1 × PBS. FISH was hybridized with a Cy3-labeled plant-telomere PNA specific probe $(TTAGGG)_3$ and Cy3-labeled *Arabidopsis* centromeres PNA probe (5-GACTCCAAAACACTA ACC-3; see the Supplemental Information). Nuclei were counterstained with

DAPI Vectashield and analyzed with a FV 1000 confocal microscope (Olympus). The DAPI image was used to define a nuclear area or ROI of each cell types to measure centromere and fluorescence intensities of the Cy3-labeled probes were measured as detailed in the Supplemental Information. Acquired images were quantified and processed using a Metamorph software package (v.6.3r6, Molecular Devices).

TRF, PETRA, Telomere Fusions, and Telomerase Activity Assays

DNA from root tips and shoots of 6-day-old was extracted by the CTAB method. TRF analysis was performed as described (Shakirov and Shippen, 2004). PETRA analysis and fusion PCR on *tert* mutants and WT Col-0 was done using 2 μg of root tip DNA as described (Heacock et al., 2004). The range of telomere length was determined using ImageQuant software. The average length of bulk telomeres was determined by ImageJ software (http://rsb.info.nih.gov/ij/). TRAP in root tips were performed as described (Kannan et al., 2008; Shakirov and Shippen, 2004).

For telomere Q-FISH quantification and statistical analysis of the data, see the Supplemental Information.

SUPPLEMENTAL INFORMATION

Supplemental Information includes Supplemental Experimental Procedures, six figures, and two movies and can be found with this article online at http://dx.doi.org/10.1016/j.celrep.2015.04.013.

ACKNOWLEDGMENTS

We thank M. Gallego for providing anti-H2AX antibodies, I. Flores and C. Vilella for help with data analysis and comments on the manuscript. This work was supported by NIH R01-GM065383 to D.E.S. Research in the M.A.B. lab is funded by European Research Council (ERC) Project TEL STEM CELL (GA#232854), European Union FP7 Projects 2007-A-20088 (MARK-AGE) and 2010-259749 (EuroBATS), Spanish Ministry of Economy and Competitiveness Projects SAF2008-05384 and CSD2007-00017, Regional of Government of Madrid Project S2010/BMD-2303 (ReCaRe), AXA Research Fund (Life Risks Project), and Lilly 2010 Preclinical Biomedicine Research Award and Fundación Botín (Spain). M.I. acknowledges support from the Spanish Ministry of Science and Innovation through grant FIS2012-37655-C02-02 and to the Generalitat de Catalunya through grant 2014 SGR 878. A.I.C.-D. is funded by the Spanish Ministry of Economy and Competitiveness (BIO2010-16673 and BIO2013-43873) and a Marie-Curie Initial Training Network (grant no. PITN-GA-2008-215118). M.-P.G.-G. was the recipient of a postdoctoral contract from BIO2010-16673 and an EMBO short-term fellowship and I.P. is funded by a JAE-CSIC PhD fellowship in the A.I.C.-D. laboratory.

Received: August 15, 2014
Revised: February 19, 2015
Accepted: April 5, 2015
Published: April 30, 2015

REFERENCES

Aida, M., Beis, D., Heidstra, R., Willemsen, V., Blilou, I., Galinha, C., Nussaume, L., Noh, Y.S., Amasino, R., and Scheres, B. (2004). The PLETHORA genes mediate patterning of the Arabidopsis root stem cell niche. Cell *119*, 109–120.

Amiard, S., Depeiges, A., Allain, E., White, C.I., and Gallego, M.E. (2011). Arabidopsis ATM and ATR kinases prevent propagation of genome damage caused by telomere dysfunction. Plant Cell *23*, 4254–4265.

Bernardes de Jesus, B., Vera, E., Schneeberger, K., Tejera, A.M., Ayuso, E., Bosch, F., and Blasco, M.A. (2012). Telomerase gene therapy in adult and old mice delays aging and increases longevity without increasing cancer. EMBO Mol. Med. *4*, 691–704.

Blasco, M.A., Lee, H.W., Hande, M.P., Samper, E., Lansdorp, P.M., DePinho, R.A., and Greider, C.W. (1997a). Telomere shortening and tumor formation by mouse cells lacking telomerase RNA. Cell *91*, 25–34.

Blasco, M.A., Lee, H.W., Rizen, M., Hanahan, D., DePinho, R., and Greider, C.W. (1997b). Mouse models for the study of telomerase. Ciba Found. Symp. *211*, 160–170, discussion 170–176.

Boltz, K.A., Leehy, K., Song, X., Nelson, A.D., and Shippen, D.E. (2012). ATR cooperates with CTC1 and STN1 to maintain telomeres and genome integrity in Arabidopsis. Mol. Biol. Cell *23*, 1558–1568.

Brady, S.M., Orlando, D.A., Lee, J.Y., Wang, J.Y., Koch, J., Dinneny, J.R., Mace, D., Ohler, U., and Benfey, P.N. (2007). A high-resolution root spatiotemporal map reveals dominant expression patterns. Science *318*, 801–806.

Cruz-Ramírez, A., Díaz-Triviño, S., Wachsman, G., Du, Y., Arteága-Vázquez, M., Zhang, H., Benjamins, R., Blilou, I., Neef, A.B., Chandler, V., and Scheres, B. (2013). A SCARECROW-RETINOBLASTOMA protein network controls protective quiescence in the Arabidopsis root stem cell organizer. PLoS Biol. *11*, e1001724.

d'Adda di Fagagna, F., Reaper, P.M., Clay-Farrace, L., Fiegler, H., Carr, P., Von Zglinicki, T., Saretzki, G., Carter, N.P., and Jackson, S.P. (2003). A DNA damage checkpoint response in telomere-initiated senescence. Nature *426*, 194–198.

De Veylder, L., Beeckman, T., Beemster, G.T., Krols, L., Terras, F., Landrieu, I., van der Schueren, E., Maes, S., Naudts, M., and Inzé, D. (2001). Functional analysis of cyclin-dependent kinase inhibitors of Arabidopsis. Plant Cell *13*, 1653–1668.

Fajkus, J., Fulnecková, J., Hulánová, M., Berková, K., Říha, K., and Matyásek, R. (1998). Plant cells express telomerase activity upon transfer to callus culture, without extensively changing telomere lengths. Mol. Gen. Genet. *260*, 470–474.

Fitzgerald, M.S., McKnight, T.D., and Shippen, D.E. (1996). Characterization and developmental patterns of telomerase expression in plants. Proc. Natl. Acad. Sci. USA *93*, 14422–14427.

Fitzgerald, M.S., Riha, K., Gao, F., Ren, S., McKnight, T.D., and Shippen, D.E. (1999). Disruption of the telomerase catalytic subunit gene from Arabidopsis inactivates telomerase and leads to a slow loss of telomeric DNA. Proc. Natl. Acad. Sci. USA *96*, 14813–14818.

Flores, I., Cayuela, M.L., and Blasco, M.A. (2005). Effects of telomerase and telomere length on epidermal stem cell behavior. Science *309*, 1253–1256.

Flores, I., Canela, A., Vera, E., Tejera, A., Cotsarelis, G., and Blasco, M.A. (2008). The longest telomeres: a general signature of adult stem cell compartments. Genes Dev. *22*, 654–667.

Fulcher, N., and Sablowski, R. (2009). Hypersensitivity to DNA damage in plant stem cell niches. Proc. Natl. Acad. Sci. USA *106*, 20984–20988.

Galinha, C., Hofhuis, H., Luijten, M., Willemsen, V., Blilou, I., Heidstra, R., and Scheres, B. (2007). PLETHORA proteins as dose-dependent master regulators of Arabidopsis root development. Nature *449*, 1053–1057.

Gan, S. (2003). Mitotic and postmitotic senescence in plants. Sci. SAGE KE *2003*, RE7.

González-García, M.P., Vilarrasa-Blasi, J., Zhiponova, M., Divol, F., Mora-García, S., Russinova, E., and Caño-Delgado, A.I. (2011). Brassinosteroids control meristem size by promoting cell cycle progression in Arabidopsis roots. Development *138*, 849–859.

Harley, C.B., Futcher, A.B., and Greider, C.W. (1990). Telomeres shorten during ageing of human fibroblasts. Nature *345*, 458–460.

Heacock, M., Spangler, E., Riha, K., Puizina, J., and Shippen, D.E. (2004). Molecular analysis of telomere fusions in Arabidopsis: multiple pathways for chromosome end-joining. EMBO J. *23*, 2304–2313.

Herbig, U., Jobling, W.A., Chen, B.P., Chen, D.J., and Sedivy, J.M. (2004). Telomere shortening triggers senescence of human cells through a pathway involving ATM, p53, and p21(CIP1), but not p16(INK4a). Mol. Cell *14*, 501–513.

Jung, P., Sato, T., Merlos-Suárez, A., Barriga, F.M., Iglesias, M., Rossell, D., Auer, H., Gallardo, M., Blasco, M.A., Sancho, E., et al. (2011). Isolation and in vitro expansion of human colonic stem cells. Nat. Med. *17*, 1225–1227.

Kannan, K., Nelson, A.D., and Shippen, D.E. (2008). Dyskerin is a component of the Arabidopsis telomerase RNP required for telomere maintenance. Mol. Cell. Biol. *28*, 2332–2341.

Lee, J.Y., Colinas, J., Wang, J.Y., Mace, D., Ohler, U., and Benfey, P.N. (2006). Transcriptional and posttranscriptional regulation of transcription factor expression in Arabidopsis roots. Proc. Natl. Acad. Sci. USA *103*, 6055–6060.

Lin, Y., and Schiefelbein, J. (2001). Embryonic control of epidermal cell patterning in the root and hypocotyl of Arabidopsis. Development *128*, 3697–3705.

Lingner, J., Cooper, J.P., and Cech, T.R. (1995). Telomerase and DNA end replication: no longer a lagging strand problem? Science *269*, 1533–1534.

López-Otín, C., Blasco, M.A., Partridge, L., Serrano, M., and Kroemer, G. (2013). The hallmarks of aging. Cell *153*, 1194–1217.

Mähönen, A.P., Bonke, M., Kauppinen, L., Riikonen, M., Benfey, P.N., and Helariutta, Y. (2000). A novel two-component hybrid molecule regulates vascular morphogenesis of the Arabidopsis root. Genes Dev. *14*, 2938–2943.

Martens, U.M., Zijlmans, J.M., Poon, S.S., Dragowska, W., Yui, J., Chavez, E.A., Ward, R.K., and Lansdorp, P.M. (1998). Short telomeres on human chromosome 17p. Nat. Genet. *18*, 76–80.

Mencuccini, M., Martínez-Vilalta, J., Vanderklein, D., Hamid, H.A., Korakaki, E., Lee, S., and Michiels, B. (2005). Size-mediated ageing reduces vigour in trees. Ecol. Lett. *8*, 1183–1190.

Petricka, J.J., Winter, C.M., and Benfey, P.N. (2012). Control of Arabidopsis root development. Annu. Rev. Plant Biol. *63*, 563–590.

Rademacher, E.H., Möller, B., Lokerse, A.S., Llavata-Peris, C.I., van den Berg, W., and Weijers, D. (2011). A cellular expression map of the Arabidopsis AUXIN RESPONSE FACTOR gene family. Plant J. *68*, 597–606.

Richards, E.J., and Ausubel, F.M. (1988). Isolation of a higher eukaryotic telomere from Arabidopsis thaliana. Cell *53*, 127–136.

Riha, K., and Shippen, D.E. (2003). Ku is required for telomeric C-rich strand maintenance but not for end-to-end chromosome fusions in Arabidopsis. Proc. Natl. Acad. Sci. USA *100*, 611–615.

Riha, K., Fajkus, J., Siroky, J., and Vyskot, B. (1998). Developmental control of telomere lengths and telomerase activity in plants. Plant Cell *10*, 1691–1698.

Riha, K., McKnight, T.D., Griffing, L.R., and Shippen, D.E. (2001). Living with genome instability: plant responses to telomere dysfunction. Science *291*, 1797–1800.

Riha, K., Watson, J.M., Parkey, J., and Shippen, D.E. (2002). Telomere length deregulation and enhanced sensitivity to genotoxic stress in Arabidopsis mutants deficient in Ku70. EMBO J. *21*, 2819–2826.

Rossi, D.J., Jamieson, C.H., and Weissman, I.L. (2008). Stems cells and the pathways to aging and cancer. Cell *132*, 681–696.

Sabatini, S., Beis, D., Wolkenfelt, H., Murfett, J., Guilfoyle, T., Malamy, J., Benfey, P., Leyser, O., Bechtold, N., Weisbeek, P., and Scheres, B. (1999). An auxin-dependent distal organizer of pattern and polarity in the Arabidopsis root. Cell *99*, 463–472.

Sarkar, A.K., Luijten, M., Miyashima, S., Lenhard, M., Hashimoto, T., Nakajima, K., Scheres, B., Heidstra, R., and Laux, T. (2007). Conserved factors regulate signalling in Arabidopsis thaliana shoot and root stem cell organizers. Nature *446*, 811–814.

Sax, K., and Enzmann, E.V. (1939). The effect of temperature on X-ray induced chromosome aberrations. Proc. Natl. Acad. Sci. USA *25*, 397–405.

Scheres, B., Benfey, P., and Dolan, L. (2002). Root development. Arabidopsis Book *1*, e0101.

Shakirov, E.V., and Shippen, D.E. (2004). Length regulation and dynamics of individual telomere tracts in wild-type Arabidopsis. Plant Cell *16*, 1959–1967.

Shakirov, E.V., Perroud, P.F., Nelson, A.D., Cannell, M.E., Quatrano, R.S., and Shippen, D.E. (2010). Protection of Telomeres 1 is required for telomere integrity in the moss Physcomitrella patens. Plant Cell *22*, 1838–1848.

Song, X., Leehy, K., Warrington, R.T., Lamb, J.C., Surovtseva, Y.V., and Shippen, D.E. (2008). STN1 protects chromosome ends in Arabidopsis thaliana. Proc. Natl. Acad. Sci. USA *105*, 19815–19820.

Surovtseva, Y.V., Churikov, D., Boltz, K.A., Song, X., Lamb, J.C., Warrington, R., Leehy, K., Heacock, M., Price, C.M., and Shippen, D.E. (2009). Conserved telomere maintenance component 1 interacts with STN1 and maintains chromosome ends in higher eukaryotes. Mol. Cell *36*, 207–218.

Thomas, H. (2013). Senescence, ageing and death of the whole plant. New Phytol. *197*, 696–711.

Tomás-Loba, A., Flores, I., Fernández-Marcos, P.J., Cayuela, M.L., Maraver, A., Tejera, A., Borrás, C., Matheu, A., Klatt, P., Flores, J.M., et al. (2008). Telomerase reverse transcriptase delays aging in cancer-resistant mice. Cell *135*, 609–622.

Truernit, E., Bauby, H., Dubreucq, B., Grandjean, O., Runions, J., Barthélémy, J., and Palauqui, J.C. (2008). High-resolution whole-mount imaging of three-dimensional tissue organization and gene expression enables the study of Phloem development and structure in Arabidopsis. Plant Cell *20*, 1494–1503.

Ubeda-Tomás, S., Federici, F., Casimiro, I., Beemster, G.T., Bhalerao, R., Swarup, R., Doerner, P., Haseloff, J., and Bennett, M.J. (2009). Gibberellin signaling in the endodermis controls Arabidopsis root meristem size. Curr. Biol. *19*, 1194–1199.

Ulmasov, T., Murfett, J., Hagen, G., and Guilfoyle, T.J. (1997). Aux/IAA proteins repress expression of reporter genes containing natural and highly active synthetic auxin response elements. Plant Cell *9*, 1963–1971.

Vera, E., and Blasco, M.A. (2012). Beyond average: potential for measurement of short telomeres. Aging (Albany, N.Y. Online) *4*, 379–392.

Vilarrasa-Blasi, J., González-García, M.P., Frigola, D., Fàbregas, N., Alexiou, K.G., López-Bigas, N., Rivas, S., Jauneau, A., Lohmann, J.U., Benfey, P.N., et al. (2014). Regulation of plant stem cell quiescence by a brassinosteroid signaling module. Dev. Cell *30*, 36–47.

Völker, A., Stierhof, Y.D., and Jürgens, G. (2001). Cell cycle-independent expression of the Arabidopsis cytokinesis-specific syntaxin KNOLLE results in mistargeting to the plasma membrane and is not sufficient for cytokinesis. J. Cell Sci. *114*, 3001–3012.

Watson, J.M., and Riha, K. (2010). Comparative biology of telomeres: where plants stand. FEBS Lett. *584*, 3752–3759.

Watson, J.M., and Riha, K. (2011). Telomeres, aging, and plants: from weeds to Methuselah - a mini-review. Gerontology *57*, 129–136.

Cell Reports

Supplemental Information

Single-Cell Telomere-Length Quantification Couples Telomere Length to Meristem Activity and Stem Cell Development in *Arabidopsis*

Mary-Paz González-García, Irina Pavelescu, Andrés Canela, Xavier Sevillano, Katherine A. Leehy, Andrew D.L. Nelson, Marta Ibañes, Dorothy E. Shippen, Maria A. Blasco, and Ana I. Caño-Delgado

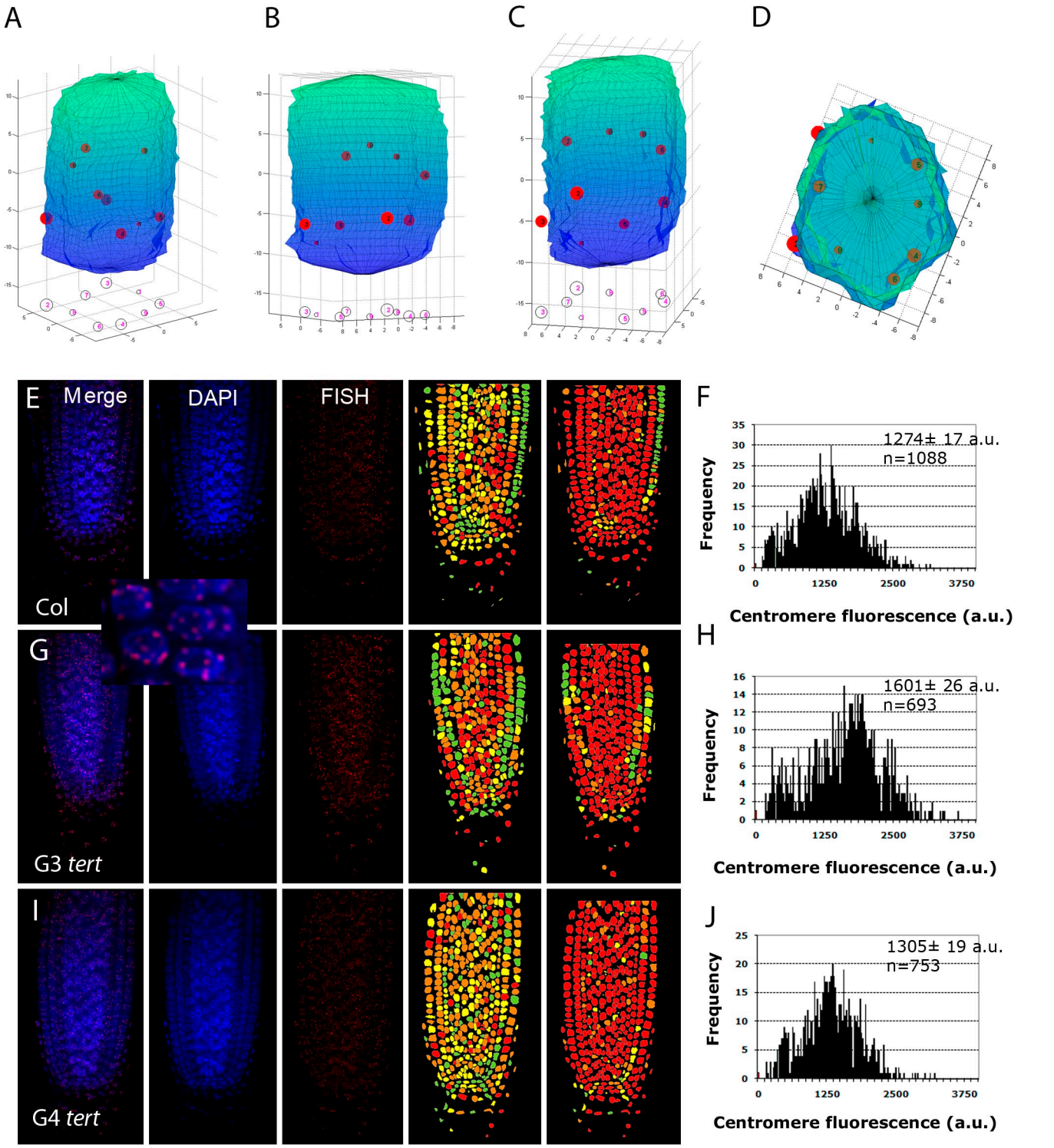
A
B
C
D
E
Merge
DAPI
FISH
Col
F
1274± 17 a.u.
n=1088
Frequency
Centromere fluorescence (a.u.)
G
G3 tert
H
1601± 26 a.u.
n=693
Frequency
Centromere fluorescence (a.u.)
I
G4 tert
J
1305± 19 a.u.
n=753
Frequency
Centromere fluorescence (a.u.)
K
% of cells within a telomere lengthper root
0-896 a.u.
896-1247 a.u
1247-2015 a.u
2015-4095 a.u
Col
G3 tert
G4 tert
L
% of cells within a telomere lengthper root
0-397 a.u.
397-575 a.u
575-1071 a.u
1071-4095 a.u
Col
G3 tert
G4 tert

Figure S1. Related to Figures 1,2. Cellular centromere distribution.

(A-D). **3D spatial localization of centromeres inside an individual cell.** (A-C) Different views of the three-dimensional model of the cell. The Z-axis corresponds to the layers of the confocal stack. The red spheres represent the centromeres detected in the layer-wise quantization process. The spheres are vertically projected onto the lower plane to provide a 2D view of the spatial distribution of the centromeres inside the cell nucleus. The diameter of the spheres is proportional to the detected size of the centromeres, whereas the spheres position along the X, Y and Z-axes corresponds to their location within the cell nucleus. (D) Zenithal view of the three-dimensional model of the cell.

(E-L). **Centromere length analysis by Q-FISH of whole-mounted roots of G3 and G4 *tert*.**

(E, G, I) Q-FISH of 6-day-old roots using a centromeric PNA probe. Centromere probe is labeled with Cy3, cell nuclei stained with DAPI and a merged image for both channels is shown (see inset). Representative centromere length pseudo-color images of WT sixday- old roots (E), G3 *tert* (G) and G4 *tert* (I) plants. Nuclei are coloured according to their average centromere fluorescence in arbitrary units.

(F, H, J) Q-FISH histograms showing centromere fluorescence frequencies in WT plants (F), G3 *tert* (H) and G4 *tert* plants (J). No statistically significant differences in centromere fluorescence were detected between WT and *tert* mutants, indicating that the differences in telomere length described in this study are not due to differences in "probe accessibility". Three independent roots were used for the analysis. n= total number of nuclei used for theanalysis. Average centromere fluorescence and SEM are indicated. (K, L) Percentage of cells showing a given fluorescence in WT, G3 *tert* and G4 *tert* plants, with percentages calculated for centromere data (K) and for telomere data (L).

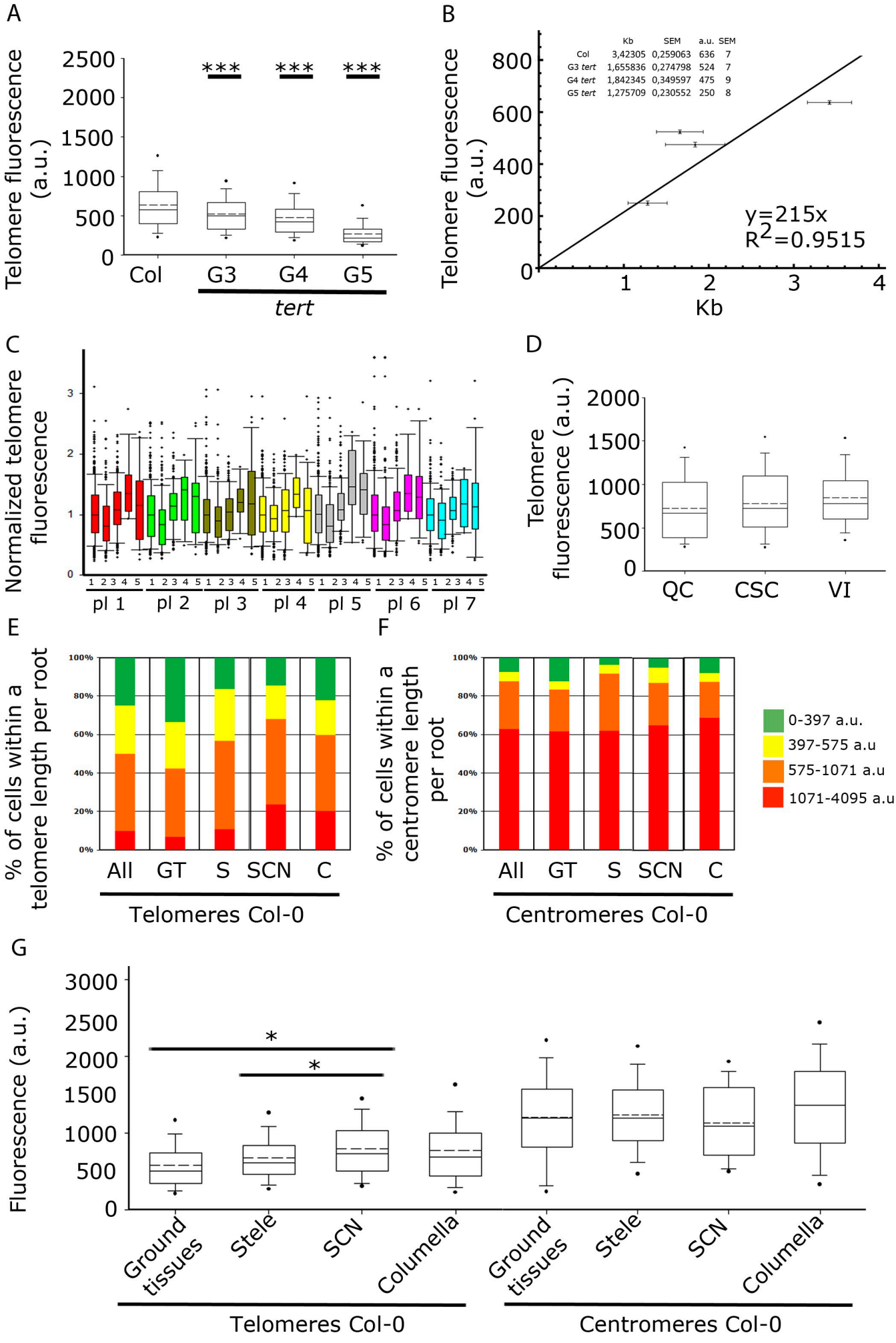
A
Telomere fluorescence (a.u.)
2500
2000
1500
1000
500
0
***
***
***
Col
G3
G4
G5
tert
B
Telomere fluorescence (a.u.)
800
600
400
200
0
Kb SEM a.u. SEM
Col 3,42305 0,259063 636 7
G3 tert 1,655836 0,274798 524 7
G4 tert 1,842345 0,349597 475 9
G5 tert 1,275709 0,230552 250 8
y=215x
R2=0.9515
1
2
3
4
Kb
C
Normalized telomere fluorescence
3
2
1
0
1 2 3 4 5
pl 1
pl 2
pl 3
pl 4
pl 5
pl 6
pl 7
D
Telomere fluorescence (a.u.)
2000
1500
1000
500
0
QC
CSC
VI
E
% of cells within a telomere length per root
100%
80%
60%
40%
20%
0%
All
GT
S
SCN
C
Telomeres Col-0
F
% of cells within a centromere length per root
100%
80%
60%
40%
20%
0%
All
GT
S
SCN
C
Centromeres Col-0
0-397 a.u.
397-575 a.u
575-1071 a.u
1071-4095 a.u
G
Fluorescence (a.u.)
3000
2500
2000
1500
1000
500
0
*
*
Ground tissues
Stele
SCN
Columella
Ground tissues
Stele
SCN
Columella
Telomeres Col-0
Centromeres Col-0

Figure S2. Related to Figures 2-4. Validation of Q-FISH technique in the Arabidopsis root.

(A) Boxplots showing the telomere length distributions in all cells of WT compared to *tert* mutants. Boxes represent the interquartile range (25^{th}-75^{th} percentiles, median indicated by the black horizontal line, average indicated by the dashed line) of the distribution, whiskers extend to the 10^{th} and 90^{th} percentiles and outliers are represented by black dots. ***p<0.001.

(B) Calibration plot to convert arbitrary units of fluorescence (a.u.) into Kb of DNA. SEM values are represented. The inset shows the table with the average telomere length expressed in kilobases (Kb) of DNA in the WT and *tert* mutants, as determined by PETRA assays, vs telomere fluorescence obtained by Q-FISH in the Arabidopsis root tips.

(C) Boxplots showing the cell type specific telomere length pattern inside each individual Col-0 plant analyzed (each color corresponds to one plant). On the Y axis are represented the raw values normalized with the median value of the telomere length distribution corresponding to all tissues, for each plant. On the X axis, 1-5 numbers stand for: 1. All tissues, 2.Ground tissues, 3. Stele, 4. SCN, 5. Columella. It can be easily observed that all plants follow the same pattern. Boxes represent the interquartile range (25^{th}-75^{th} percentiles, median indicated by the black horizontal line, average indicated by the dashed line) of the distribution, whiskers extend to the 10^{th} and 90^{th} percentiles and outliers are represented by black dots. *p<0.05.

(D) Boxplots showing the telomere length distributions in the quiescent centre (QC), columella stem cells (CSC) and vascular initials (VI) of Col-0 roots. No statistical differences were observed.

(E-F) Col-0 percentage of cells within a telomere and centromere length interval for each cell type. All=all tissues, GT=ground tissues, S=stele, SCN=stem cell niche, C=columella

(G) Boxplots showing the heterogeneity between cell types in telomere length distributions compared to centromere length distribution. Boxes represent the interquartile range (25^{th}-75^{th} percentiles, median indicated by the black horizontal line, average indicated by the dashed line) of the distribution, whiskers extend to the 10^{th} and 90^{th} percentiles and outliers are represented by black dots. *p<0.05.

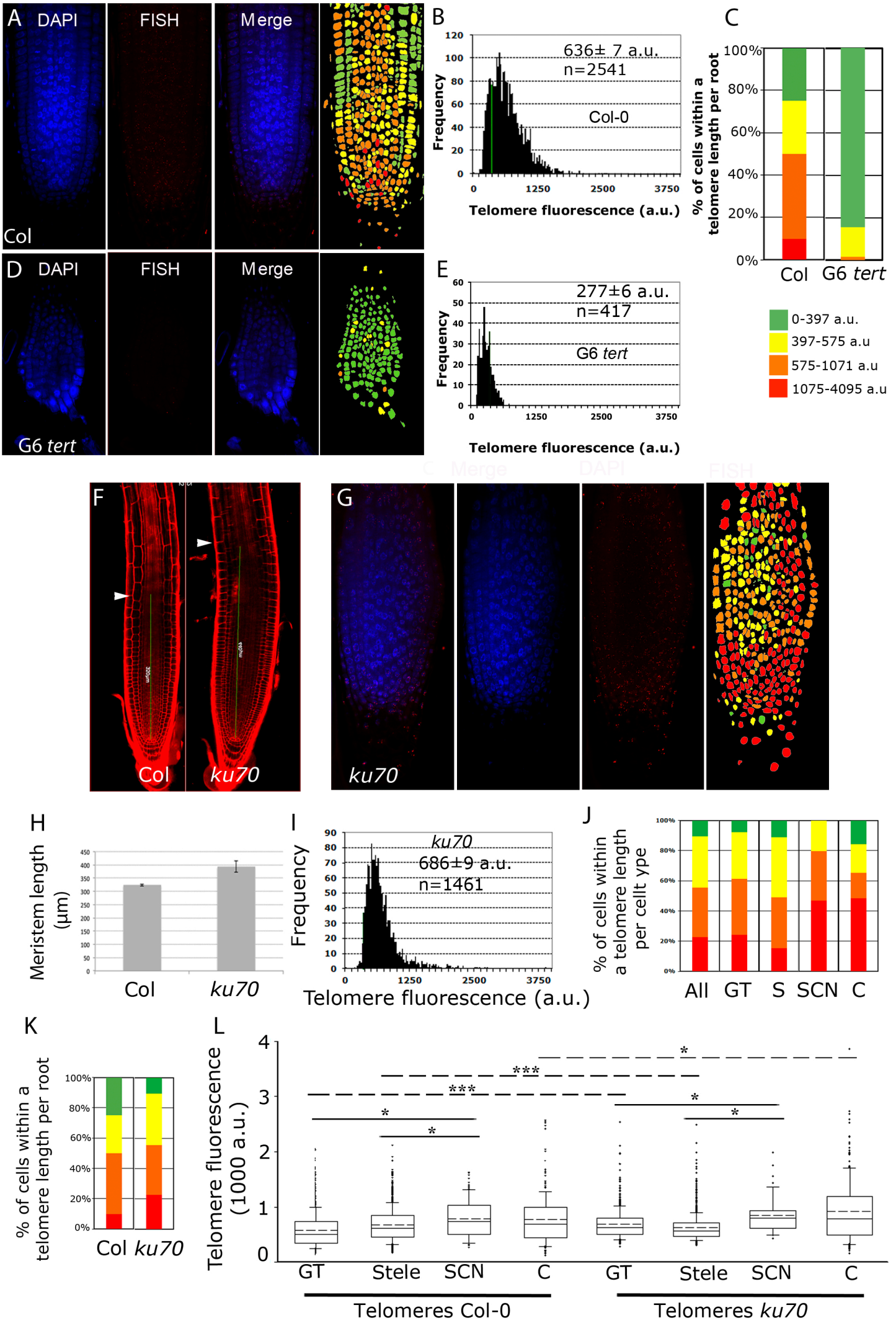
A DAPI
FISH
Merge
Col
B
636± 7 a.u.
n=2541
Col-0
Frequency
Telomere fluorescence (a.u.)
C
% of cells within a telomere length per root
Col
G6 tert
0-397 a.u.
397-575 a.u
575-1071 a.u
1075-4095 a.u
D DAPI
FISH
Merge
G6 tert
E
277±6 a.u.
n=417
G6 tert
Frequency
Telomere fluorescence (a.u.)
F
Col
ku70
G
ku70
H
Meristem length (µm)
Col
ku70
I
ku70
686±9 a.u.
n=1461
Frequency
Telomere fluorescence (a.u.)
J
% of cells within a telomere length per cellt ype
All
GT
S
SCN
C
K
% of cells within a telomere length per root
Col
ku70
L
Telomere fluorescence (1000 a.u.)
GT
Stele
SCN
C
Telomeres Col-0
Telomeres ku70

Figure S3. Related to Figures 2-4. Telomere-length analysis by whole-mounted root Q-FISH of telomere defective mutants.

(A-E). **G6 *tert* mutant analysis.** (A,D) Q-FISH in WT six-day-old roots (A), and G6 *tert* plants (D) telomeric PNA probe stained with Cy3, cell nuclei stained with DAPI and a merged image for both channels. Representative telomere length pseudo-color images of WT and G6 *tert* plants. Nuclei are colored according to their average telomere fluorescence in arbitrary units. (B,E) Telomere Q-FISH histograms showing telomere fluorescence frequencies in WT (B) and G6 *tert* (E) roots. Average telomere fluorescence, SEM and the number of nuclei n are indicated. (C) Percentage of cells showing a given fluorescence in WT and G6 *tert*. Note that *tert* mutants are enriched in cells with the shortest telomeres (green color).

(F-L). Phenotypic analysis and telomere length gradients of *ku70* mutants.

(F) Confocal images of six-day-old WT and *ku70* mutants roots stained with PI. Arrows mark the boundary between the proximal meristem and the elongation zone of the root. Scale bars: 100 μm. (G) Representative telomere length pseudo-color images of in *ku70* six-day-old roots. (H) The meristem length of 6-day-old roots of *ku70* mutants compared to WT. Asterisks indicate significant differences relative to WT for each day. (I) Telomere Q-FISH histograms showing telomere fluorescence frequencies in *ku70* roots. Average telomere fluorescence, SEM and the number of nuclei n, pooled form 3 plants, are indicated. (Note that *ku70* mutants are enriched in cells with longest telomeres (red and orange color). (J) *ku70* percentage of cells within a telomere length interval for each cell type. All=all tissues, GT=ground tissues, S=stele, SCN=stem cell niche, C=columella. (K) Percentage of cells showing a given fluorescence in WT and *ku70*. (L) Boxplots showing telomere length distributions of Col-0 cell types compared to *ku70*. Boxes represent the interquartile range (25^{th}-75^{th} percentiles, median indicated by the black horizontal line, average indicated by the dashed line) of the distribution, whiskers extend to the 10^{th} and 90^{th} percentiles and outliers are represented by black dots. Black lines represent internal comparisons between Col-0 cell types and *ku70* cell types, with significant differences between SCN and ground tissues and between SCN and stele in both cases. Dashed lines represent comparisons between corresponding cell types in Col-0 and *ku70*. Telomere lengths in columella cells and ground tissues in ku70 were larger than their correspondent cell types in Col-0, meanwhile the telomeres in stele were shorter, with an overall telomere length larger in *ku70* compared to Col-0. ***$p<0.001$ *$p<0.05$.

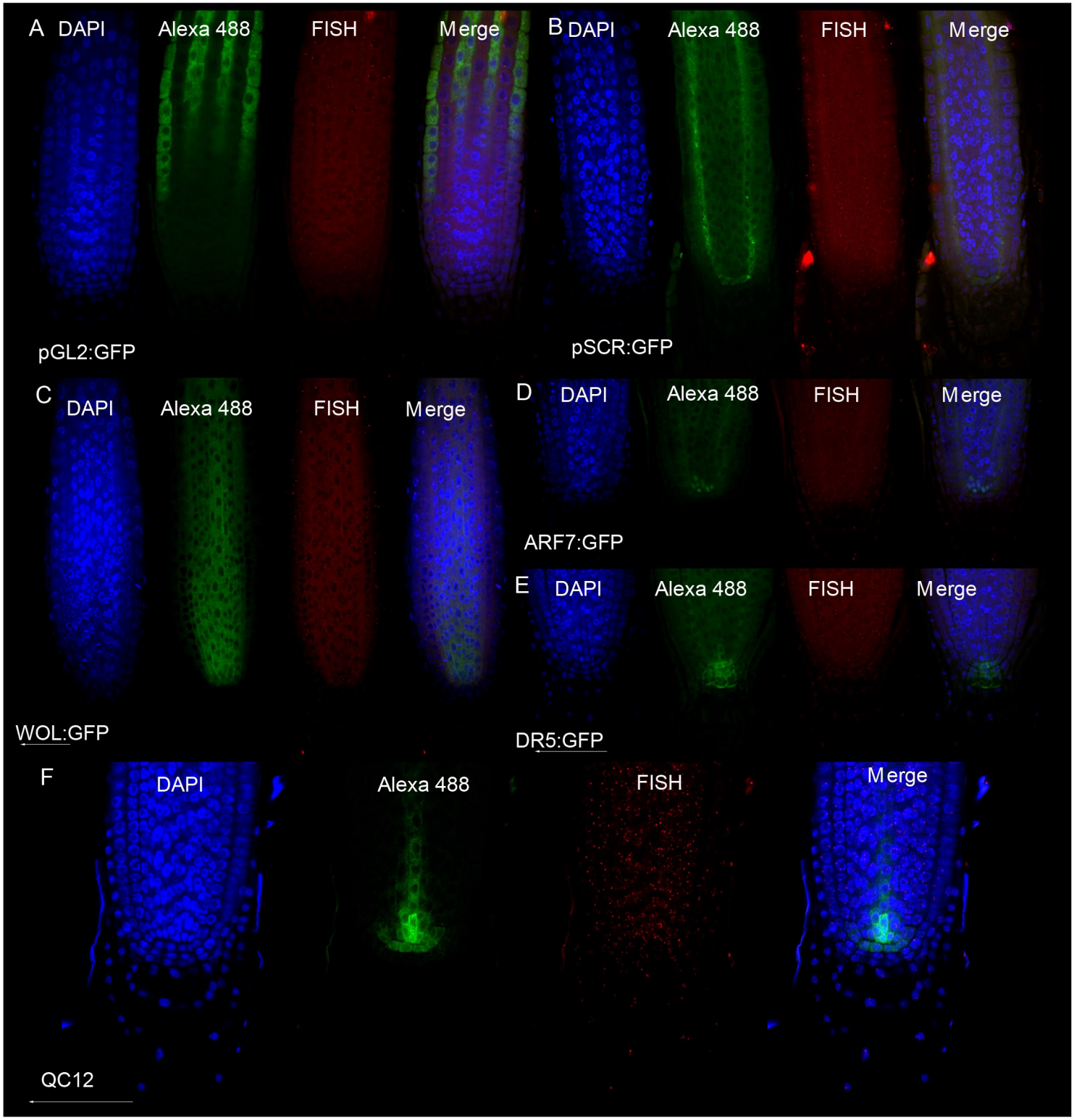
A DAPI
Alexa 488
FISH
Merge
pGL2:GFP
B DAPI
Alexa 488
FISH
Merge
pSCR:GFP
C DAPI
Alexa 488
FISH
Merge
WOL:GFP
D DAPI
Alexa 488
FISH
Merge
ARF7:GFP
E DAPI
Alexa 488
FISH
Merge
DR5:GFP
F
DAPI
Alexa 488
FISH
Merge
QC12

Figure S4. Related to Figure 3. Markers for root compartments. (A-F) Immunostaining using anti-GFP antibodies preceded telomere Q-FISH and enabled the distinction of several root cellular domains. Hair epidermis (*pGL2:GFP*) (A), endodermis-quiescent center (*pSCR:GFP*) (B), stele (*pWOL:GFP*) (C), columella and QC (DR5:GFP) (D), vascular initials (*pARF7:ARF7:GFP*) (E) and QC with vascular initials (QC12) (F).

A

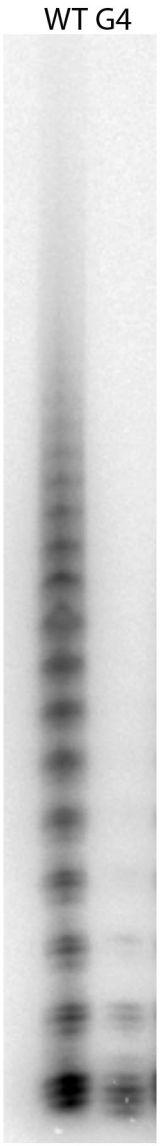
WT G4

B

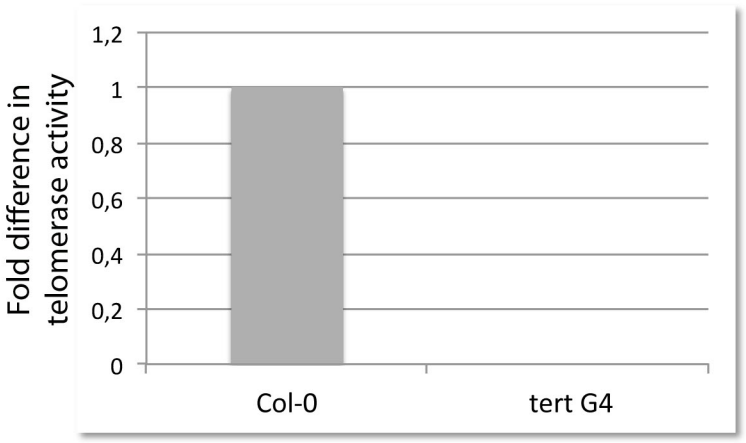
Fold difference in telomerase activity
1,2
1
0,8
0,6
0,4
0,2
0
Col-0
tert G4

C

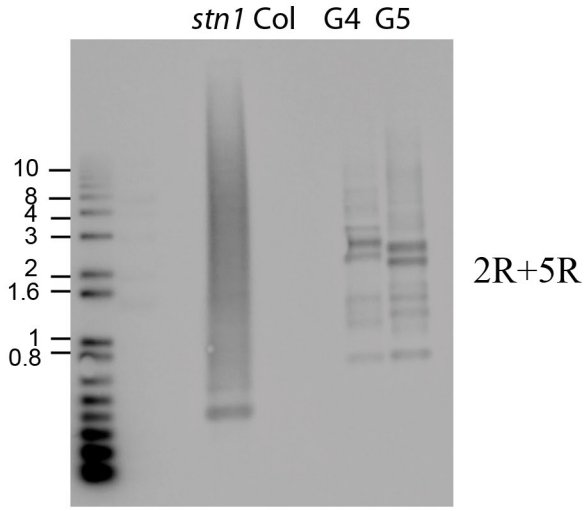
stn1 Col G4 G5
10
8
4
3
2
1.6
1
0.8
2R+5R

D

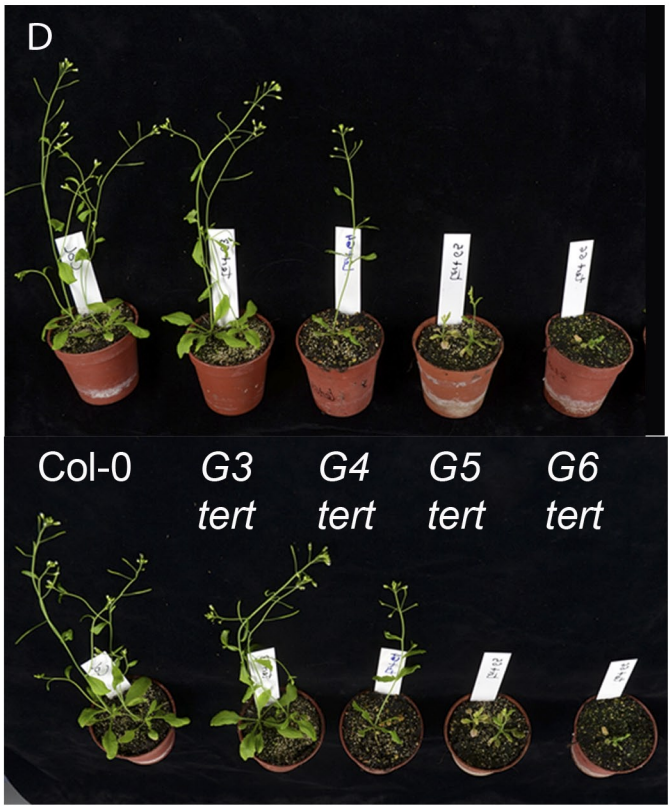
Col-0
G3 tert
G4 tert
G5 tert
G6 tert

Figure S5. **Related to Figures 2,4. TRAP (A) and Q-TRAP (B) analysis in the root tips in WT and G4 *tert* mutants**.

(C) Telomere fusion PCR analysis of *tert* and *stn1* (positive control) are shown. Primers specific for 2R and 5R were used using sectioned Arabidopsis root tips.

(D) Arabidopsis WT and *tert* mutants grown in long day conditions on soil for 3 weeks. Mutants display developmental defects and the progressive depletion of proliferative capacity.

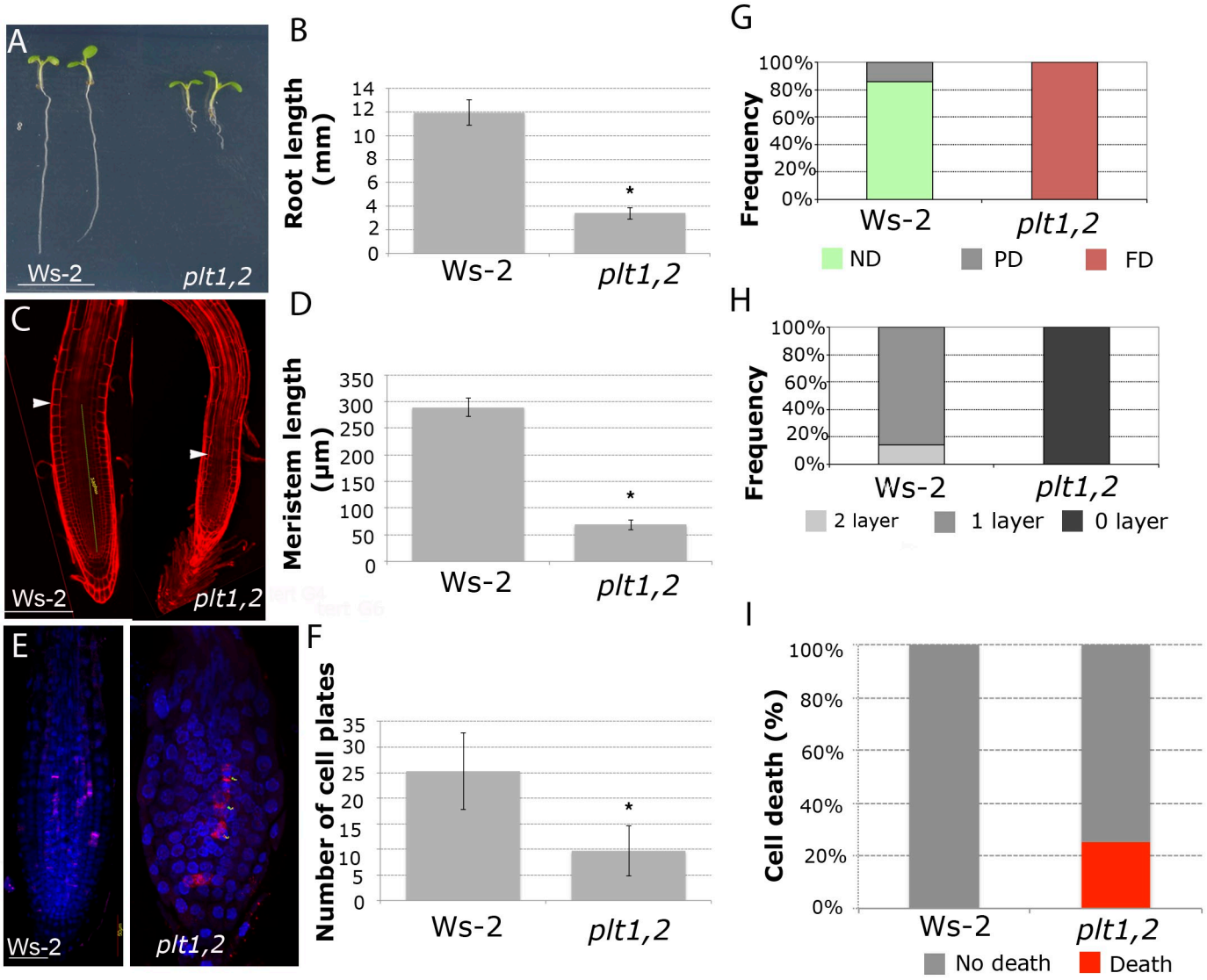
A
Ws-2
plt1,2
B
Root length (mm)
14
12
10
8
6
4
2
0
*
Ws-2
plt1,2
G
Frequency
100%
80%
60%
40%
20%
0%
Ws-2
plt1,2
ND
PD
FD
C
Ws-2
plt1,2
D
Meristem length (µm)
350
300
250
200
150
100
50
0
*
Ws-2
plt1,2
H
Frequency
100%
80%
60%
40%
20%
0%
Ws-2
plt1,2
2 layer
1 layer
0 layer
E
Ws-2
plt1,2
F
Number of cell plates
35
30
25
20
15
10
5
0
*
Ws-2
plt1,2
I
Cell death (%)
100%
80%
60%
40%
20%
0%
Ws-2
plt1,2
No death
Death

Figure S6. Related to Figure 6. Six-day-old phenotypes of *plt1 plt2* roots.

(A) Morphology of six-day-old seedlings of Ws-2 and *plt1 plt2* plants. Scale bar: 10 mm.

(B) Root-length measurements of Ws-2 and *plt1 plt2* seedlings compared to WT. Asterisks denote statistically significant differences relative to WT. (P<0.001)

(C) Confocal images of six-day-old Ws-2 and *plt1 plt2* roots stained with PI. Arrows mark the boundary between the proximal meristem and the elongation zone of the root. Scale bars: 100 μm.

(D) The meristem length of 6-day-old roots Ws-2 and *plt1 plt2* compared to WT. Asterisks indicate significant differences to the WT for each day. (P<0.001).

(E) Whole-mount immunofluorescence with anti-KNOLLE antibodies (Volker et al., 2001) in 6-day-old roots Ws-2 and *plt1 plt2*. Scale bar: 50μm.

(F) Number of cell plates calculated in whole-mount immunofluorescence with anti-KNOLLE antibodies present in Ws-2 and *plt1 plt2*. Asterisks denote a statistically significant difference with WT (P<0.001).

(G) Frequency distribution of QC division in Ws-2 and *plt1 plt2* seedlings compared to Col-0 (WT) at 6 days after germination. PD=partially divided, ND=non-divided, FD=fully divided.

(H) Frequency distribution of the number of cell layers is given between the QC and the first differentiated columella cells that contain starch granules in Ws-2 and *plt1 plt2* seedlings. Note in *plt1 plt2* mutants all (100%) of CSC differentiated.

(I) Cell death in the meristem was measured for intense propidium-iodide (PI) staining to count dead stem cells per root in Ws-2 and *plt1 plt2*.

SUPPLEMENTAL MOVIE LEGENDS

Movie S1. Related to Figure 1. Confocal optical sections of a 6-day-old Arabidopsis root. Z-stack confocal optical sections at 0.8μm spacing were collected from 6-day-old roots. Immunofluorescence of GFP expressing cells in WOX5:GFP, telomere fluorescence obtained by Q-FISH along the root using a PNA probe stained with Cy3 and cell nuclei stained with DAPI.

Movie S2. Related to Figure 2. 3D reconstruction of single root cells revealing the topology of the fluorescence spots. Desktop recording of the 3D cell model creation process. The user is first prompted to select the cell to be rendered in 3D. Together with the segmentation process that allows detecting the boundaries of the cell nucleus in each stack layer, the layer-wise quantization process is conducted on the cell of choice applying an adaptive fluorescence sensitivity threshold. As a result, the 3D model of the cell is computed and presented to the user, who can freely rotate the cell to study its internal topology.

SUPPLEMENTAL EXPERIMENTAL PROCEDURES

Telomere-length quantification and statistical analysis of the data

After acquisition in the confocal microscope, the 3 channels images were passed to our custom semi-automatic Matlab program in order to generate the binary mask containing nuclear areas, based on the blue channel (DAPI) (Supporting Information). For final adjustments (final separation of nuclei that were still united) the binary masks were manually processed in Adobe Photoshop CS5 (version 12.0.4, Adobe Systems Incorporated). During this process, the original 8-bit image containing both DAPI and Cy3 channels was used as background and the binary mask obtained in Matlab was used as a layer on top of the background. By changing the transparency of the layer it was possible to visualize all the telomeres and to improve the mask ensuring that all telomeres fall inside their nuclear area.

Once the final binary mask was generated, it was introduced together with the Cy3 image (red channel) in the Metamorph software package (version 6.3r6, Molecular Devices, Union City, CA, USA) to identify and measure telomeres/centromeres intensity inside nuclear area.

The Granularity Metamorph module was used to identify telomeres/centromeres spots and remove background. This measured the intensity of each telomere/centromere inside each nucleus avoiding changes in ploidy or area (Supporting Information). Based on the average telomere/centromere intensity per nucleus, a coloured map was generated and the intensity data for each analysed plant was saved as Excel files for histogram generation and further processing.

Telomere data from WT plants (7 independent roots) were compared with telomere data from G3 *tert* (3 independent roots), G4 *tert* (3 independent roots) and G5 *tert* (3 independent roots) using Kruskal-Wallis One Way Analysis on Ranks test. In all cases significant differences with $P<0.001$ were obtained.

The same statistical test was used for centromeres and telomeres-centromeres data comparisons and also for comparisons between cell types.

Root length and meristem length were measured in at least three independent experiments. Roots were scanned and measured with ImageJ software (http://rsb.info.nih.gov/ij/). For comparisons, Student's *t*-tests were performed in all cases.

The folowing steps were folowed to set up the quantification of fluorescence probes:

1. Generation of a Binary mask from the confocal microscopy images

1.1. Select the file of interest and open it with Olympus FV 1000.

1.2. Save all 8 and 16 bit images.

1.3. For 8 bit images: In Output Format, select Merge Channel (using assigned LUT), Merge Method: Amount, Channel Selection: 1 and 2 corresponding to DAPI (nuclei) and Cy3 (telomeres/centromeres).

1.4. For 16 bit images: In Output Format, select Raw data Extracted (without LUT), Extract Method: Raw (16 bit TIFF), Channel Selection: 1 and 2 (corresponding to DAPI and Cy3).

1.5. Select the Z-plane of interest (containing the middle plane of the root corresponding to the QC) with FV1000.

1.6. The 8 and 16 bit folders contain all the images saved at step 1.3 and 1.4 .

1.7. The folder “mask” will be described in the following steps, in section 2.

2. Nuclei segmentation process (Matlab)

As a result, the typical appearance of the Arabidopsis roots images captured by the confocal microscope is the one presented in Figure 1.

Due to the confocal microscopy capture technique employed, the cell nuclei appear in the blue channel and the telomeric information in the red channel in an 8 bit image. Therefore, a simple channel separation allows obtaining the nuclear area of the root.

As the construction of telomapping requires analyzing cells individually, it becomes necessary to **create a binary mask** that allows isolating each cell from the remaining ones. The automatic construction of such a binary mask is a challenging task, as the objects to segment (i.e. cells nuclei) present fairly distinct gray levels across the image. There is little that can be done in this regard, as these differences are due to the cylindrical geometry of the root, which causes some cells to be more illuminated than others.

Despite this fact, we have opted for the use of histogram based segmentation techniques (i.e. based on setting a gray level threshold for dividing the image into foreground -cells- and background –non-cells) for obtaining the binary mask in this stage of the imaging analysis module development. The motivation for this decision is that these approaches are at the same time simple and adaptable.

The described method has been implemented using Matlab Release 2008a, as a command-line application that allows users tuning its parameters. Subsequently, the resulting binary mask is displayed and the user has the option of saving it into an image file. Running on a standard PC (Intel Core Duo@1.83GHz, 2 GB RAM), the processing of a good resolution image (e.g. 1024x768 pixels or similar) takes less than five seconds.

After testing several segmentation methods, the most accurate one has proved to be a two-step segmentation strategy that combines average filtering based adaptive thresholding segmentation and morphological operators:

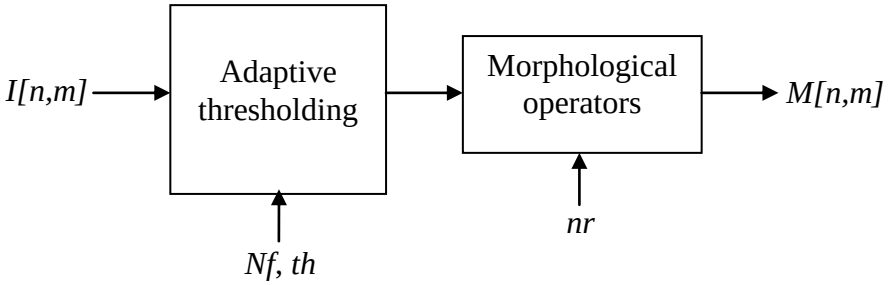

The general idea is to create a first version of the binary mask by means of average filtering based adaptive thresholding, and subsequently improving the quality of the mask through the use of morphological operators, aiming at reducing its noise level.

The rationale behind average filtering adaptive thresholding is based on segmenting the image using a locally computed gray level threshold (Wellner, 1993). By proceeding this way, we set a segmentation threshold, which is highly local, thus being fairly immune to the large illumination variations found across the image. To that end, the image is filtered using an averaging filter of size *Nf* x *Nf* pixels (see equation 1). As a result, we obtain an averaged version of the image, where each pixel equals the mean gray level of its *Nf*-sized square neighborhood.

$$I_{avg}[n,m] = I[n,m] * h_{Nf}[n,m], \quad where\ h_{Nf}[n,m] = \frac{1}{Nf^2}\begin{pmatrix} 1 & \cdots & 1 \\ \vdots & \ddots & \vdots \\ 1 & \cdots & 1 \end{pmatrix} \qquad (1)$$

Next, a segmentation decision step based on a sensitivity threshold *th* is conducted (see equation 2), which consists of setting each pixel to white in case it is a *th* percent darker than the average gray level of its neighbors (Wellner, 1993)

.

$$I_{bin}[n,m] = \begin{cases} 0, if\ \ I[n,m] < th \cdot I_{avg}[n,m] \\ 1, if\ \ I[n,m] \geq th \cdot I_{avg}[n,m] \end{cases} \qquad (2)$$

In equations 1 and 2, $I[n,m]$, $I_{avg}[n,m]$, $I_{bin}[n,m]$ refer to the original image, the image resulting from the averaging filtering and the thresholded image, respectively, $h_{Nf}[n,m]$ represents the impulse response of the *Nf* x *Nf* averaging filter, and * stands for the linear convolution operation. It is worth mentioning that the *Nf* and *th* parameters are tunable by the user.

After this process is completed, the binary image $I_{bin}[n,m]$ is an approximate mask which is somewhat noisy, and sometimes tends to present overlapping cells nuclei.

At its current stage of development, cell overlapping can only be solved by means of manual post processing. However, we can alleviate much of the burden of this process by applying morphological operators, aiming to improve the overall quality of the final binary mask ($M[n,m]$). To that end, two morphological operators are sequentially applied: majority and horizontal breaking.

The application of the first morphological operator is intended to reduce noisy pixels (i.e. fairly isolated white pixels that do not belong to cells nuclei). Basically, what the majority morphological operator does is setting a pixel to white if five or more pixels in its 3-by-3 neighborhood are white; otherwise, it sets the pixel to black (see equation 3). Therefore, this allows eliminating isolated (i.e. noisy) white pixels resulting from the adaptive thresholding stage.

$$I_{maj}[n,m] = \begin{cases} 0, \textit{if} \sum_{k=n-1}^{n+1} \sum_{l=m-1}^{m+1} I_{bin}[k,l] < 5 \\ 1, \textit{if} \sum_{k=n-1}^{n+1} \sum_{l=m-1}^{m+1} I_{bin}[k,l] \geq 5 \end{cases} \qquad (3)$$

The amount of noise reduction can be increased by the cascaded application of the majority morphological operator. The number of times it is applied determines the noise reduction (*nr*) input parameter that appears in the two-step segmentation strategy, also tunable by the user.

However, the amount of noise reduction achievable through this method has a natural threshold, as after a certain number of iterations this morphological operation becomes idempotent (Gonzalez, 2008). Therefore, care must be taken when setting the *nr* parameter, as a too large value will uselessly increase the computational complexity of the noise reduction process.

Finally, after the noise reduction step, an H-break morphological operator is applied in order to split cells in case they are connected by one pixel, which renders the final mask, *M[n,m]*.

$$M[n,m] = H_{break}\{I_{maj}[n,m]\} \qquad (4)$$

Results

In order to analyze the influence of setting the neighborhood parameter *Nf* to different values, we used different neighborhood sizes (*Nf*=20, 40 and 80) with a fixed threshold (*th*=1%) value.

Almost all the cells in the image were recovered, and no geometric artifacts appeared. Moreover, small neighborhood sizes tended to yield oversegmented and noisy masks. On the other hand, if the neighborhood is large, cells tend to overlap. Bearing this in mind, and considering that the cells nuclei average size is around 40 pixels, setting *Nf*=40 seems a neat decision, which is backed up by empirical evidence.

Next, we set the threshold at different levels (*th*=1%, 10% and 20%) for a fixed neighborhood size (*Nf*=40). The higher the threshold the more undesired information (i.e. background) is retrieved. Empirical evaluation yielded the best results by setting *th* equal to 1.

Finally, the application of the majority and H-break morphological operators aim at reducing the level of noise in the mask obtained from the previous stage. We varied the noise reduction parameter (*nr*) to different values and we observed that the more number of times the majority morphological operator is applied, the greater noise reduction is achieved. Empirical experimentation suggested that the *nr* parameter should be set to 10 or 15, depending on the sample.

It is important to mention that the resulting mask (Fig. 1) needs some manual processing (basically separating overlapped nuclei, holes filling and contour delimitation) in order to obtain the final result.

Due to the high complexity of the sample and the big number of nuclei, the mask automatically generated by Matlab (Fig. 1) was transferred to Adobe Acrobat 9 Professional (CS5) for further manual processing (better separation of joint nuclei and better delimitation of the nuclei contour). During this process, the original 8 bit image containing both DAPI and Cy3 channels was used as background and the binary mask obtained in Matlab was used as a layer on top of the background. By changing the transparency of the layer it was possible the visualization and the inclusion of all the telomeres inside their nuclear area.

3. Metamorph analysis

The 16 bit sets of confocal images were analyzed in Metamorph (version 7.7.0.0, Molecular Devices, Union City, CA, USA). The final mask generated in Photoshop was auto-thresholded for light objects and transformed into a 1-bit binary image. The

morphology filter Fill holes was applied to 1-bit binary image in order to fill the holes corresponding to nucleolus inside each nucleus, generating the Holes image. Granularity module was applied to the Cy3 16 bit image to identify only telomeres (min width 3.5, max width 10, Intensity Above Local Background 50) or centromeres (min width 5, max width 20, Intensity Above Local Background 50) and to assign a value of 0 to the intensity of all the remaining pixels. In this way we efficiently removed any background present in the image. The generated image was titled Granules. The parameters used for Granularity module were set after several measurements of individual telomeres/centromeres size in pixels and the difference in intensity between a real telomere/centromere and the local background. Furthermore, the accuracy of the identification was visually checked in the original image after applying the module.

The Granules image was binarized, combined with the original Cy3 image through LOGICAL AND arithmetical function and thresholded, to create an image with the original grey values of the granules which was called AND. The contours of all the nuclei (regions) in Holes image were transferred to AND image to identify only the telomeres/centromeres inside nuclear areas. Cy3 fluorescence of individual telomeres was measured as ¨Average grey value¨ units (arbitrary units of fluorescence) using the Integrated Morphometry Analysis module and given as the average intensity/nucleus (the sum of all the telomeres/centromeres inside a nuclear area divided by the number of telomeres/centromeres in that area). Telomeric/centromeric intensity values obtained in this way were exported to Excel for frequency histograms generation and further analysis.

In order to visualize and classify the nuclei according to their telomeric intensity, Configure Object Classifier module was used and a code of four colours (green, yellow, orange and red), representing the nuclei having the intensity in the 25^{th}, 50^{th} and 90^{th} quartiles was generated. These intervals were established based on all WT data (7 plants for telomeres and 3 plants for centromeres) and maintained constant for all the analyzed mutants to facilitate comparisons.

Protocol for Metamorph Analysis:

3.1. Open final mask generated in Photoshop-> Auto-threshold for light objects-> 1-Bit binary image

3.2. Process menu->Morphology filters->Fill Holes (1-Bit binary image). Apply ->Holes image

3.3. **Apps -> Granularity (Cy3 image)-> Min width 3,5 max 10 background 50 (for centromeres Min width 5 max 20 background 50). Apply**

3.4. Create a blank 16 bit image to be used to mark nuclei. The easiest way is to use Arithmetic (process menu) to multiply the Cy3 image by 0 and create a 16 bit result. The result image is called Multiply.

3.5. The Granules image should be made into a binary image by using a threshold of 1 – 4095 and then Binarize (Binary Operations, Process menu)

3.6. Use Logical AND to create an image with the original grey values of the granules. Arithmetic dialog (Process menu): Source Image 1 – Original image (Cy3), Source 2-Image – binary result from step 1, Result Bit Depth – whatever the original image was (16bit), Operation – Logical AND.

3.7. Set threshold for the result of step 4 (AND) grey values > 0.

3.8. You can measure the result of step 5 with Integrated Morphometry Analysis (Measure menu) to get the number of granules, the grey values for each granules and the summary for the measurements. In Integrated Morphometry Analysis window, in Preferences, click Measure All regions.

3.9. You can measure the granules specific to each nucleus using the following method.

3.10. **Open Holes**

3.11. Create Regions Around Objects (Regions menu)

3.12. Transfer regions of interest from Holes to the results of step 5 (AND) (granules having the initial grey value and thresholded). Select “All regions”.

3.13. Measure using Integrated Morphometry Analysis (Measure menu). Only objects within <u>all</u> of the regions of interest (overlapping the holes) will be measured. In Integrated Morphometry Analysis window, in Preferences, click Measure All regions. Also, if you log the Summary Data each region of interest will be logged separately.

3.14. Generating the Excel file which contains the Region Name ,the Average intensity coming from all the points in that region, the area and the count (name of the file_total):

3.14.1. Measurements- Avg int and Total int

3.14.2. Summary-Configure Log- Click only the options Region Name and Average- OK

3.14.3. Open Log- F9-Log Data

3.14.4. Save as name of file_total.xls

3.14.5. Measure with Integrated Morphometry Analysis the image Holes. Measurements – Total area.

3.14.6. Object data. Open Log- F9-Log Data.

3.14.7. Measure with Integrated Morphometry Analysis the image AND Measurements- Avg int and Total int

3.14.8. Summary-Configure Log- Click only Region Name and Count- OK

3.14.9. Open Log- F9-Log Data

3.14.10. Change total intensity by count in the head of the column

3.14.11. Sort all data by Average intensity and remove all the regions with 0 avg int.

3.14.12. Sort the remaining data by Total area of the region and select only the regions which are above 100 area.

Observation: Step 8.12 can be skiped if we are interested only in obtaining the average intensity per nucleus and not the intensity value of each particle.

3.15. Each nucleus can be measured by itself using the following method.

3.16. Save an Integrated Morphometry Analysis state file (Measure menu) that measures the Average Intensity and turns Off the preference to *Measure all regions*. **** It has to be done only once, at the begging

3.17. Save an Integrated Morphometry Analysis state file (Measure menu) that measures the Average Intensity and turns Off the preference to *Measure all regions*. **** It has to be done only once, at the begging

3.18. How to do it: In the IMA window: a) Measurements-> Click only Average intensity; b) Preferences-> Unclick *Measure all regions*; c) Save State->OK-> Save as Average intensity.IMA

3.19. Load the State saved before (Average intensity.IMA)

3.20. In Summary->Open Log. Do not press F9 : Log the data

3.21. Pause logging to the Summary Log (Log menu, Summary sub-menu-> Pause Summary Log)

3.22. Selecting the image result of step 9 (AND with all the Regions) -> Journal menu->Loop sub-menu->Loop for all regions ->Image AND, Select Journal-> Journal_to_loop.jnl

3.22.1. Loop through all regions in an image *Journal to Loop (saved as Journal_to_loop.jnl)*

3.22.2. Select one region in AND to activate it. Measure AND using Integrated Morphometry Analysis (Measure menu). Only objects within the active region of interest will be measured.

3.22.3. Log the Summary Data (Press Record button) for the region of interest (it will not go to the spreadsheet or file because logging was paused on step 15).

3.22.4. Journal menu-> Variables-> Assign variable -> Under Variable and Expression, assign to the variable *Average* the measurement variable *IMASummary.Average*. Press OK.

3.22.5. Transfer the active region of interest from the current image (AND) to Multiply (the blank 16 bit image result of step 2). Select *Clear regions from Destination before transfer* and *Active Region*.

3.22.6. Select the region in *Multiply* (Journal menu, Recording tools->Select Region->Select) to make the transferred region active.

3.22.7. Paint the region from step E. Display menu, Graphics sub-menu-> Paint Region-> Paint Mode: Inside region area; Paint Color: Value from variable, Variable Name: *Average*.

3.23. Clear the regions from the image result of step F (Multiply).

3.24. This image now has objects with grey values equal to the average of the granule grey values.

3.25. Multiply->Threshold-> Inclusive, from 1 to the highest intensity

3.26. Measure Multiply with IMA (Average intensity and Total area) and log the results in an excel file After, unclick Total Area and leave only Avg intensity. If not, in Config Object Classifier it will always activate as a filter Total Area too.

3.27. Select Multiply image->Measure menu-> Morphometry-> Configure Object Classifier: Classifiers (from b to e). Click Active for each of them and set the Filter Range and color:

3.28. In Telomeres case : b) 0-397, Green; c) 397-575, Yellow; d) 575-1071, Orange; e) 1071-4095, Red.

3.29. Click Recalc after setting each of them. Filters: Average gray value

3.30. Observation: Select the image, Measure menu-> Morphometry-> Measure Objects and Load set File-> and click Recalc. It goes faster.

3.31. Select Multiply image->Measure menu-> Morphometry-> Measure Objects-> Resulting image=Measured Multiply --- This image has the colors according to the average intensity of each nucleus.

3.32. Save Multiply and Measured Multiply images in the folder .

4. Excel and statistical analysis

The results generated in Metamorph were first filtered by total area size in order to eliminate all the ROIs that have an area smaller than 100 pixels^2 (the smallest area that a real nucleus can have). In this way, only real nuclei will contribute to the final fluorescence results.

Based on this data, frequency histograms were generated and the 25th, 50th and 90th quartiles were calculated in Excel, generating color coded percentiles graphs which served for further comparison between samples.

Kruskal-Wallis One Way Analysis of Variance on Ranks test was used to evaluate the differences between unpaired samples after all samples failed the Shapiro-Wilk

normality test. Both tests were performed using SigmaPlot`s (Systat Software, Inc.) statistical package.

Telomere data from WT plants (7 plants) was compared with telomere data from *tert* G3 (3 plants), *tert* G4 (3 plants) and *tert* G5 (3 plants) mutants. In all cases significant differences with $p<0.05$ were obtained. The same statistical test was used for centromeres data comparisons and telomeres-centromeres comparisons ($p<0.001$. To make the comparisons between cell types, first we measured telomere fluorescence for each cell type in each sample being analyzed. Next, we gathered the results from all the samples in one phenotype and generated the final data for each cell type for each phenotype. Given that all data failed the Shapiro-Wilk normality test, we compared each cell type with the others (ground tissues vs stele, SCN and columella, stele vs ground tissues, SCN and columella, SCN vs columella) by using the Kruskal-Wallis One Way Analysis of Variance on Ranks in SigmaPlot.

5. Kbs to a.u.f conversion

In order to convert kbs into a.u.f., the values of a.u.f. measured by Q-FISH corresponding to Col-0 and G3-G5 tert mutants were plotted against the values in kbs measured by PETRA again for Col-0 and G3-G5 tert mutants and set to pass through origin (0 a.u.f. correspond to 0 kbs). LinearModelFit function (Mathematica, Wolfram Research) was used to fit a linear polynome to the data, using the standard error of the mean (s.e.m) values to compute the weights as 1/ (s.e.m)^2. The value obtained for the slope gives an approximation for the number of a.u.f corresponding to 1 kb, with $R^2=0.9516$.

SUPPLEMENTAL REFERENCES

Gonzalez, R.C. and Woods, R.E. a. (2008). *Digital Image Processing, 3rd ed.* Prentice-Hall.

Wellner, P. (1993). *Adaptive Thresholding for the DigitalDesk. Techical Report EPC-93-110.* Cambridge, UK: Rank Xerox Research Center.